



Biomechanically driven flow of a magnetohydrodynamic bio-fluid in a micro-vessel with slip and convective boundary conditions

K. Ramesh¹ · N. S. Akbar² · M. Usman³

Received: 27 April 2018 / Accepted: 8 May 2018 / Published online: 15 May 2018
© Springer-Verlag GmbH Germany, part of Springer Nature 2018

Abstract

The main objective of the present study is to model the peristaltic transport of an incompressible couple stress fluid in an inclined asymmetric channel under the impact of porous medium, inclined magnetic field, heat and mass transfer. The effects of viscous dissipation, thermal radiation, Joule heating, chemical reaction, slip and convective boundary conditions are also taken into account. The entropy generation analysis is also studied. The non-dimensional and non-linear partial differential equations that govern the fluid flow model are simplified under the long wavelength and low Reynolds number assumptions. The entropy generation number due to heat transfer, fluid friction and magnetic field is formulated. The exact solutions for the stream function, pressure gradient, temperature, concentration, heat transfer coefficient and Nusselt number are derived. The trapping phenomenon is also presented for different wave shapes through streamline patterns. The comparison has been made with the results obtained in the symmetric and asymmetric channel, and Newtonian and couple stress fluid model. The results indicate that the entropy generation number achieves higher values in the region close to the walls of the channel, while it gains low values near the center of the channel. Temperature is a decreasing function of radiation parameter, Prandtl number and thermal Biot number. The size of the trapped bolus is greater in the Newtonian fluid model than the couple stress fluid model.

1 Introduction

The study of fluid flow in a uterus is important in reproductive physiology to understand how a fertilized embryo is carried to the implant site. There are different mechanisms of fluid motion inside the uterus, most important is the one due to the myometrial contractions. The flow of intra-uterine fluid in a non-pregnant myometrium is due to two types of contractions at different phases of menstrual cycles. The first type produces wave-like contractions

called uterine peristalsis and the other type is sustained contractions. These myometrial contractions may occur in both symmetric and asymmetric directions (Narayan and Goswamy 1994). The study of peristaltic propulsion has become popular among the researchers during the last five decades because of its vital and extensive applications in physiology and industry. In physiology, the peristaltic mechanism is considered to be a major source of transport of various biological fluids from one place to another place in the human body. Examples of this mechanism in physiology are the transport of chyme in the gastrointestinal tract, Cilia motion, movement of spermatozoa, vasomotion of small blood vessels (i.e., venules, arterioles, capillaries), and urine transport from kidney to the bladder. This mechanism is also involved in plant physiology, in particular it governs phloem translocation by driving a sucrose solution along tubules by peristaltic contractions. In industry, many devices have been introduced that work on the mechanism of peristalsis. For instance, hose pump, finger pump, heart-lung machine, blood pump, roller pump and dialysis machine, these are very useful in transporting sensitive and corrosive fluids. This mechanism was first introduced by Latham (1966). He carried out theoretical

✉ K. Ramesh
ramesh.katta1@gmail.com

N. S. Akbar
noreensher@yahoo.com

M. Usman
musman1@dayton.edu

¹ Department of Mathematics, Lovely Professional University, Jalandhar 144411, India

² Department of Mathematics, DBS&H CEME National University of Sciences and Technology, Islamabad, Pakistan

³ Department of Mathematics, University of Dayton, Dayton, USA

and experimental research to understand the phenomenon of peristalsis in the ureteral functions. After his pioneering experiments, many researchers have examined the peristaltic flow in various situations. Fung and Yih (1968) described the most important phenomenon of reflux. Vesicoureteral reflux (VUR) is the backward flow of urine from the bladder into the kidneys. The muscles of the bladder and ureter along with the pressure of urine in the bladder prevent urine from flowing backward through the ureter. VUR allows the bacteria, which may be present in the urine inside the bladder, to reach the kidneys. This can lead to kidney infection, scarring and damage. Gastroesophageal reflux disease (GERD) is commonly experienced in the patient who is suffering with heartburn and regurgitation. GERD can also frequently occurs in women during pregnancy (Turan et al. 2016). This is because the bigger the baby gets, the more pressure it exerts on the stomach and lower esophageal sphincter. Due to this reason, the reflux symptoms may be increased. Some of the relevant studies can be seen in the references (Shapiro 1967; Anggiansah et al. 1994) and the references therein. Intra-uterine fluid motion induced by peristaltic contractions of the uterine muscles play an important role in the initial process of human reproduction. It accelerates the transport of spermatozoa towards the fallopian tube where fertilization occurs. After fertilization it is responsible for embryo transport to a successful site of implantation. Several models have been proposed to describe the peristaltic flow in many physiological vessels (e.g., ureter or vas deferens), where contraction of concentric muscles induce symmetric trains of wall displacement waves along the vessel. Asymmetric contractions may exist along the walls of a two-dimensional channel, when displacement waves on the upper and lower walls move independently with a phase shift between them. Eytan and Elad (1999) have investigated the wall-induced peristaltic fluid flow in two-dimensional channel with wave trains having a phase difference moving independently on the upper and lower walls to simulate intra-uterine fluid motion in a sagittal cross-section of the uterus. In view of these applications in physiology, many authors have reported their research contribution in the direction of asymmetric peristaltic mechanism with different fluids by using various analytical, numerical, and experimental methods under different conditions with reference to physiological and mechanical situations. Recent investigations in this direction can be seen in the references (Reddy et al. 2007; Ali and Hayat 2008; Srinivas and Pushparaj 2008; Nadeem and Akram 2010) and some more references therein.

The effects of magnetohydrodynamics in the peristalsis play an important role in areas of medical sciences. Examples of such areas include magneto therapy, hyperthermia, arterial flow, compressor, optimization of blood

pump machine, magnetic endoscopy, constipation treatment, gastrogenic pathology, cancer tumor treatment causing hyperthermia, bleeding reduction during surgeries and targeted transport of drug using magnetic particles as drug carries. The concept of magnetohydrodynamics is also useful in magnetic resonance imaging (MRI), when a patient undergoes in a static magnetic field. Magnetohydrodynamics is also applicable in various engineering problems such as, electromagnetic casting, liquid metal cooling of nuclear reactors, continuous casting process of metals and plasma confinement (Bhatti and Abbas 2016). Magnetohydrodynamics is based on the fact that the interaction of magnetic field and electric current generates a repulsive force. If this happens in a fluid it can propel the fluid in a direction perpendicular to both the field and the current. Due to this reason, magnetohydrodynamics is also used in the study of electrically conducting fluids such as electrolytes, saltwater, liquid metals and plasmas. The controlled application of low intensity and frequency pulsating fields modify the cell and tissue. Magnetic susceptibility of chyme is satisfied by the ions contained in the chyme. The magnetic field could cause heat inflammations, ulceration, and many diseases of uterus and bowel. Due to these substantial facts, a peristaltic flow of non-Newtonian fluids under the influence of a magnetic field has become very important and gained the attention of researchers. Nadeem and Akram (2010) have investigated the influence of inclined magnetic field on the peristaltic flow of a Williamson fluid in an inclined asymmetric channel under lubrication approach. They have used perturbation and numerical methods to solve the simplified problem. Akbar (2015) presented the exact solutions of the influence of magnetic field on peristaltic flow of a Casson fluid model under the long wavelength and low Reynolds number approximations. Abd-Alla and Abo-Dahab (2015) have studied the peristaltic flow of a Jeffrey fluid in an asymmetric rotating channel utilizing long wavelength and low Reynolds number assumptions. Bhatti et al. (2016) have discussed the effects of variable magnetic field on the peristaltic flow of Jeffrey fluid in a non-uniform rectangular duct having compliant walls using long wavelength and low Reynolds number assumptions. They have obtained the exact solutions of non homogeneous governing equations through eigenfunction expansion method. The flow of non-Newtonian fluids through porous medium is a topic of great interest due to its applications in engineering, geo-fluid dynamics and biomechanics. In biological systems such flows can be observed in kidneys, lungs, small blood vessels, cartilage and bones. The tissues of the human body can be regarded as deformable porous media. Some other applications included are polymer technology, the mechanics of cochlea in the human ear, physiology, orthopedics, blood flow and cardiology. The study of

porous medium can help in examining the flow in a vessel when the luminal surface of endothelial layer is attached with glycocalyx, which contains a series of micro-molecules and adsorbed plasma proteins (Maiti and Misra 2012). In the realm of physiological fluid dynamics, it is often required to have an estimate of a variety of fluid mechanical variables when some physiological fluid has to pass through porous structures. Due to this and its wide range of applications, many researchers have modelled the flow of different fluids through porous media [see the references (Elshehawey et al. 2006; Maiti and Misra 2011; elmaboud and Mekheimer 2011; Tripathi et al. 2015) and some more references there in].

Heat transfer phenomenon has wide range of applications in industrial and engineering processes including nuclear reactor cooling, space cooling, energy production, biomedical sciences. For example, in hemodialysis and oxygenation, it is used to obtain information about the properties of tissues, hypothermia treatment, sanitary fluid transport, blood pump in heart-lung machines, transport of corrosive fluids, laser therapy and coldness cryosurgery, as a mean to destroy undesirable tissues, including cancer. Heat transfer involves many complicated processes in tissues such as heat conduction, heat convection due to blood flow through tissue pores, metabolic heat generation and external interactions such as, electromagnetic radiation emitted from electronic devices (Khaled and Vafai 2003). Many conventional fluids such as water, ethylene glycol and engine oil may impose restrictions in several thermal processes due limited capabilities in terms of thermal properties. Moreover, most solids in particular metals, have one to three times higher thermal conductivities than conventional fluids. The fluids consisting of solid particles have enhanced thermal conductivities. The blood flow rate can be approximated by a technique in which heat is produced locally or injected and the thermal clearance is monitored (Hayat et al. 2015). Blood carries a large quantity of heat to different parts of the body. In view of these applications, researchers have studied the heat transfer effects in the peristalsis. For instance, Akbar and Nadeem (2011) have presented a perturbation solutions for the peristaltic flow of a Jeffrey-six constant fluid in a non-uniform tube under the assumptions of long wavelength and low Reynolds number. Akram and Nadeem (2013) have discussed the peristaltic motion of a two dimensional Jeffrey fluid in an asymmetric channel under the effects of induced magnetic field and heat transfer. They have obtained the exact and closed form Adomian solutions under the long wavelength and low Reynolds number approximation. Akbar (2015) has given the exact analytical solution for the peristaltic flow in a tube with entropy generation and energy conversion rate. Hayat et al. (2016) have analyzed the magneto hydrodynamic peristaltic

transport of Prandtl fluid in a channel with flexible walls using large wavelength and small Reynolds number assumptions. Recently, the study of entropy generation has become a topic of interest for numerous researchers due to its extensive use in heat exchangers, electronic cooling, turbo machinery, solar collectors, chemical vapor deposition instruments and combustions. In view of this, the improvement of thermal systems has gained a notable consideration. Thermal systems have been analyzed by employing the second law of thermodynamics. According to the second law of thermodynamics the accessible energy is always demolished mostly or absolutely and terminated quantity of energy is proportional to the entropy production. The execution of thermal gadgets is continuously transformed by irreversible dissipation that leads to an expansion of entropy and decline of thermal proficiency. Along these facts, the entropy generation decays or minimizes the decimation of energy identification with the best productive energy framework plan. In engineering and industrial systems there are several references for entropy generation (Hayat et al. 2017). Heat transfer, viscous dissipation, radiation and electrical conduction are the basic sources of entropy generation in thermal systems. Bejan (1980, 2001) explained the different constructive factors beyond the entropy generation in applied engineering, where spoliation of available work of a system exists throughout the entropy creation, and reviewed the entropy generation minimization of flow configurations in engineering flow systems. In view of this, several researchers (Srinivasacharya and Hima 2016; Basak et al. 2012) have studied the irreversibility shapes and entropy generation for different geometries. Mass transfer refers to the movement of mass from one location/component to another. In a variety of engineering processes, mass transfer is of common occurrence. Particularly, in the field of chemical engineering, the study of mass transfer is of vital importance, more specifically in the branches of heat transfer engineering, separation process engineering and reaction engineering. The rate at which mass transfer takes place depends on flow pattern and diffusivity (Misra et al. 2018).

The combined effect of heat and mass transfer is very useful in chemical industry and in reservoir engineering due to thermal recovery process and may be found in salty springs in the sea. Heat and mass transfer effects are quite prevalent in hemodialysis, oxygenation and nutrients diffuse out of the blood vessels to the neighboring tissues, design of chemical processing equipment, formation and dispersion of fog, damage of crops due to freezing, food processing, cooling towers, distribution of temperature and moisture over grove fields (Raissi et al. 2016). Due to aforesaid applications, many researchers have focused their attention in the field of peristalsis with the effects of heat

and mass transfer. Hina et al. (2012) have worked on the fundamental problem of peristalsis with heat and mass transfer in the presence of a chemical reaction under the long wavelength, low Reynolds number and small Grashof number approximations. Tripathi (2013) presented an analytical and computational studies on the transient peristaltic heat flow through a finite length porous channel under the assumptions of low Reynolds number and long wavelength. Hayat et al. (2016) have addressed the mixed convective peristaltic flow of Carreau-Yasuda fluid bounded in a compliant wall channel. Hayat et al. (2016) have dealt with the influence of inclined magnetic field on peristaltic flow of an incompressible Williamson fluid in an inclined channel with heat and mass transfer. Bhatti et al. (2017) have analyzed heat and mass transfer with the transverse magnetic field on the peristaltic motion of two-phase flow (particle fluid suspension) through a planar channel.

The theory of couple stress fluids by Stokes (1966), considers the couple stresses in addition to the classical Cauchy stress. This simplest generalization of the classical fluid theory also allows polar effects such as the presence of couple stresses and body couples. When additives are mixed in the fluids (such as lubricants, oils and greases), the forces present in the fluids oppose the forces of additives. This opposition makes a couple force. This force induces a couple stress in the fluid/lubricant. The couple stress fluid model is capable of describing various complex fluids including liquid crystals, polymeric suspensions that have long chain molecules, animal and human blood, infected urine and many lubricants (Ramesh 2016). Due to these exciting applications, many researchers have made their contributions in different flow problems of couple stress fluid in various situations [see the references (Adesanya et al. 2015; Ramesh 2016) and some more references therein]. The aforementioned works have been presented for mathematical models consisting of non-linear differential equations and linear boundary conditions as a result of no-slip conditions. It is widely accepted that no-slip condition in polymeric liquids with high molecular weight is not appropriate and fails in many problems like thin film problems, rarefied fluid problems, fluid motion inside the human body and flow on multiple interfaces. It is also known that slip effects may appear for two types of fluids such as rarefied gases and fluids with elastic characteristics. In such fluids, slippage appears as a result of large tangential traction. It is clear from few experiments that the occurrence of slippage is possible in the non-Newtonian fluids (i.e. polymer solution and molten polymer). In general, in the study of fluid–solid surface interactions, the concept of slip of a fluid at a solid wall serves to describe macroscopic effects of certain molecular phenomena. In many applications, the flow pattern corresponds to a slip

flow, the fluid presents a loss of adhesion at the wetted wall, making the fluid slide along the wall (Tripathi and Beg 2015). The fluids that exhibit slip effect have many applications for instance, the polishing of artificial heart valves and internal cavities (Ellahi et al. 2012). A little research has been done by the researchers in the direction of peristaltic problems with the slip conditions. In view of this, recently many researchers are focused their attention on the peristaltic fluid flow problems using slip boundary conditions. For instance, Akbar and Nadeem (2012) have discussed the peristaltic flow of an incompressible six constant Jeffrey's fluid model under the long wavelength and low Reynolds number approximations. Shit et al. (2016) have developed a mathematical model for the peristaltic transport of magnetohydrodynamic flow of bio-fluids through a micro-channel with rhythmically contracting and expanding walls under the influence of an applied electric field. Javed et al. (2016) have attempted the problem to address the peristaltic transport of Walters-B fluid in a compliant wall channel. Some more recent relevant studies can be found in the references (Shit and Ranjit 2016; Hayat et al. 2016; Ellahi et al. 2015, 2016; Bhatti et al. 2016; Akbarzadeh et al. 2016; Tripathi and Beg 2014; Shirvan et al. 2017; Bhatti et al. 2017) and the references therein.

It is well known fact that, many ducts in physiological systems are neither horizontal nor vertical but have some inclination with the axis. Entropy generation for the peristaltic flows has not gained much attention by researchers. With this and aforesaid motivations in mind, the aim of the present analysis is to discuss the entropy generation on the peristaltic flow in an inclined asymmetric channel under the various effects such as, inclined magnetic field, porous medium, Joule heating, chemical reactions, slip and convective boundary conditions. The entropy generation number due to heat transfer, radiation, magnetic field, heat generation and fluid friction is formulated. Using long wavelength and low Reynolds number approximations we have simplified the governing equations. The exact solutions for the velocity, pressure gradient, temperature and concentration profiles are obtained. The effects of pertinent parameters in the present model have been shown through the graphs.

2 Mathematical formulation and solution

We consider the peristaltic flow of incompressible non-Newtonian fluid (couple stress fluid model) in an infinite two-dimensional inclined asymmetric channel of width $H_1 + H_2$. The channel asymmetry is produced due to the channel having different phase difference and amplitudes. The channel is considered with the inclination angle ζ to the horizontal axis. We choose Cartesian coordinate system

in such a way that X -axis is taken along the axial direction and Y -axis is transverse direction of the flow. The flow is governed by the sinusoidal waves with different amplitudes and phases moving at a constant speed c along with the walls of the channel. The fluid is electrically conducting in the presence of an applied uniform magnetic field B_0 making an angle β^* with the vertical axis. The effects of induced magnetic field is negligible due to small magnetic Reynolds number. The fluid flow is considered through homogeneous porous medium. The wall configuration is such that H_1 and H_2 represent the positions of upper and lower walls of the channel respectively. The geometry of the wall surfaces is defined as

$$H_1(X, t) = d_1 + a_1 \cos\left(\frac{2\pi}{\lambda}(X - ct)\right), \tag{1}$$

$$H_2(X, t) = -d_2 - a_2 \cos\left(\frac{2\pi}{\lambda}(X - ct) + \phi\right), \tag{2}$$

where a_1 and a_2 are the wave amplitudes, λ is the wavelength, c is the velocity of propagation, t is the time and X is the direction of wave propagation. The phase difference ϕ varies in the range $0 \leq \phi \leq \pi$, in which $\phi = 0$ corresponds to symmetric channel with waves out of phase and $\phi = \pi$ corresponds to that with waves in phase, and further a_1, a_2, d_1, d_2 and ϕ meet the following relation $a_1^2 + a_2^2 + 2a_1a_2 \cos \phi \leq (d_1 + d_2)^2$.

In the fixed frame, the continuity, momentum, energy and concentration equations for an incompressible magnetohydrodynamic couple stress fluid through porous medium in an inclined peristaltic channel in the presence of inclined magnetic field, in the absence of body couples are

$$\nabla \cdot \mathbf{V} = 0, \tag{3}$$

$$\rho \frac{D\mathbf{V}}{Dt} = -\nabla P + \mu \nabla^2 \mathbf{V} - \eta \nabla^4 \mathbf{V} + \mathbf{J} \times \mathbf{B} + \mathbf{R} + \rho g(\sin \zeta \hat{i} - \cos \zeta \hat{j}), \tag{4}$$

$$\rho c_p \frac{DT}{Dt} = k^* \nabla^2 T + \Phi - \frac{\partial q_r}{\partial Y} + \frac{1}{\sigma} \mathbf{J} \cdot \mathbf{J} + Q_0, \tag{5}$$

$$\frac{DC}{Dt} = D \nabla^2 C + \frac{DK_T}{T_m} \nabla^2 T - k(C - C_0), \tag{6}$$

in which, \mathbf{R} is the Darcy’s resistance in the porous medium, is given by

$$\mathbf{R} = -\frac{\mu}{k_0} (U \hat{i} + V \hat{j}), \tag{7}$$

an inclined magnetic field of strength B_0 has the following form

$$\mathbf{B} = (B_0 \sin \beta^*, B_0 \cos \beta^*, 0), \tag{8}$$

the current density \mathbf{J} expression is given by

$$\mathbf{J} = \sigma(\mathbf{V} \times \mathbf{B}). \tag{9}$$

The above equation and the Eq. (8) yield

$$\mathbf{J} = \sigma B_0 (U \cos \beta^* - V \sin \beta^*), \tag{10}$$

$$\mathbf{J} \times \mathbf{B} = -\sigma B_0^2 \cos \beta^* (U \cos \beta^* - V \sin \beta^*) \hat{i} + \sigma B_0^2 \sin \beta^* (U \cos \beta^* - V \sin \beta^*) \hat{j}. \tag{11}$$

The expression for the Joule heating can be written in the form

$$\frac{1}{\sigma} \mathbf{J} \cdot \mathbf{J} = \sigma B_0^2 (U^2 \cos^2 \beta^* + V^2 \sin^2 \beta^* - 2UV \sin \beta^* \cos \beta^*), \tag{12}$$

the viscous dissipation Φ satisfy the following equation

$$\Phi = \mu \left[2 \left\{ \left(\frac{\partial U}{\partial X} \right)^2 + \left(\frac{\partial V}{\partial Y} \right)^2 \right\} + \left(\frac{\partial U}{\partial Y} + \frac{\partial V}{\partial X} \right)^2 \right] + \eta \left[\left(\frac{\partial^2 U}{\partial X^2} + \frac{\partial^2 U}{\partial Y^2} \right)^2 + \left(\frac{\partial^2 V}{\partial X^2} + \frac{\partial^2 V}{\partial Y^2} \right)^2 \right], \tag{13}$$

and the radiative heat flux q_r satisfies

$$q_r = -\frac{4\sigma^* \partial T^4}{3\alpha^* \partial Y}. \tag{14}$$

Assuming the temperature difference within the flow to be small and expanding T^4 about T_0 by Taylor series, we have

$$T^4 \cong 4T_0^3 T - 3T_0^4, \tag{15}$$

combining the Eqs. (14) and (15), radiative heat flux q_r can be written as

$$q_r = -\frac{16\sigma^* T_0^3 \partial T}{3\alpha^* \partial Y}, \tag{16}$$

where \mathbf{V} is the velocity field, ρ is the fluid density, D / Dt represents the material time derivative, t is the time, P is the pressure, μ is the dynamic viscosity, η is material constant associated with couple stresses, g is the acceleration due to the gravity, \hat{i} and \hat{j} are the unit vectors, c_p is the specific heat at constant pressure, T is the temperature, k^* is the thermal conductivity, σ is the electrical conductivity of the fluid, Q_0 is the constant heat generation parameter, C is the concentration, D is the coefficient of mass diffusivity, K_T is the thermal diffusion ratio, T_m is the mean temperature, k is the chemical reaction parameter, k_0 is the permeability of porous medium, U and V are the components of velocity along X and Y –directions respectively, β^* is the inclination angle of magnetic field, σ^* denotes the Stefan–Boltzmann constant and α^* the mean absorption coefficient.

Using the Eqs. (7), (11), (13) and (16), in the Eqs. (3)–(6), the equations of the present problem become

$$\frac{\partial U}{\partial X} + \frac{\partial V}{\partial Y} = 0, \quad (17)$$

$$\begin{aligned} \rho \left(\frac{\partial U}{\partial t} + U \frac{\partial U}{\partial X} + V \frac{\partial U}{\partial Y} \right) &= -\frac{\partial P}{\partial X} + \mu \left(\frac{\partial^2 U}{\partial Y^2} + \frac{\partial^2 U}{\partial X^2} \right) \\ &- \eta \left(\frac{\partial^4 U}{\partial X^4} + 2 \frac{\partial^4 U}{\partial X^2 \partial Y^2} + \frac{\partial^4 U}{\partial Y^4} \right) \\ &- \sigma B_0^2 \cos \beta^* (U \cos \beta^* - V \sin \beta^*) - \frac{\mu}{k_0} U + \rho g \sin \zeta, \end{aligned} \quad (18)$$

$$\begin{aligned} \rho \left(\frac{\partial V}{\partial t} + U \frac{\partial V}{\partial X} + V \frac{\partial V}{\partial Y} \right) &= -\frac{\partial P}{\partial Y} + \mu \left(\frac{\partial^2 V}{\partial Y^2} + \frac{\partial^2 V}{\partial X^2} \right) \\ &- \eta \left(\frac{\partial^4 V}{\partial X^4} + 2 \frac{\partial^4 V}{\partial X^2 \partial Y^2} + \frac{\partial^4 V}{\partial Y^4} \right) \\ &+ \sigma B_0^2 \sin \beta^* (U \cos \beta^* - V \sin \beta^*) - \frac{\mu}{k_0} V - \rho g \cos \zeta, \end{aligned} \quad (19)$$

$$\begin{aligned} \rho c_p \left(\frac{\partial T}{\partial t} + U \frac{\partial T}{\partial X} + V \frac{\partial T}{\partial Y} \right) &= k^* \left(\frac{\partial^2 T}{\partial X^2} + \frac{\partial^2 T}{\partial Y^2} \right) \\ &+ \mu \left[2 \left\{ \left(\frac{\partial U}{\partial X} \right)^2 + \left(\frac{\partial V}{\partial Y} \right)^2 \right\} + \left(\frac{\partial U}{\partial Y} + \frac{\partial V}{\partial X} \right)^2 \right] \\ &+ \eta \left[\left(\frac{\partial^2 U}{\partial X^2} + \frac{\partial^2 U}{\partial Y^2} \right)^2 + \left(\frac{\partial^2 V}{\partial X^2} + \frac{\partial^2 V}{\partial Y^2} \right)^2 \right] \\ &+ \sigma B_0^2 (U^2 \cos^2 \beta^* + V^2 \sin^2 \beta^* - 2UV \sin \beta^* \cos \beta^*) \\ &+ \frac{16\sigma^* T_0^3}{3\alpha^*} \frac{\partial^2 T}{\partial Y^2} + Q_0, \end{aligned} \quad (20)$$

$$\begin{aligned} \left(\frac{\partial C}{\partial t} + U \frac{\partial C}{\partial X} + V \frac{\partial C}{\partial Y} \right) &= D \left(\frac{\partial^2 C}{\partial X^2} + \frac{\partial^2 C}{\partial Y^2} \right) \\ &+ \frac{DK_T}{T_m} \left(\frac{\partial^2 T}{\partial X^2} + \frac{\partial^2 T}{\partial Y^2} \right) - k_1 C. \end{aligned} \quad (21)$$

The appearance of static and wave structures is connected by the subsequent associations

$$\begin{aligned} x = X - ct, y = Y, u(x, y) &= U(X, Y, t) - c, v(x, y) \\ &= V(X, Y, t), p(x, y) = P(X, Y, t), \end{aligned} \quad (22)$$

where u , v and p are velocity components and pressure in the wave frame respectively.

The Eqs. (17)–(21), under the relations (22) convert to the wave frame and these are given by

$$\frac{\partial u}{\partial x} + \frac{\partial v}{\partial y} = 0, \quad (23)$$

$$\begin{aligned} \rho \left(u \frac{\partial u}{\partial x} + v \frac{\partial u}{\partial y} \right) &= -\frac{\partial p}{\partial x} + \mu \left(\frac{\partial^2 u}{\partial x^2} + \frac{\partial^2 u}{\partial y^2} \right) \\ &- \eta \left(\frac{\partial^4 u}{\partial x^4} + 2 \frac{\partial^4 u}{\partial x^2 \partial y^2} + \frac{\partial^4 u}{\partial y^4} \right) \\ &- \sigma B_0^2 \cos \beta^* [(u + c) \cos \beta^* - v \sin \beta^*] \\ &- \frac{\mu}{k_0} (u + c) + \rho g \sin \zeta, \end{aligned} \quad (24)$$

$$\begin{aligned} \rho \left(u \frac{\partial v}{\partial x} + v \frac{\partial v}{\partial y} \right) &= -\frac{\partial p}{\partial y} + \mu \left(\frac{\partial^2 v}{\partial x^2} + \frac{\partial^2 v}{\partial y^2} \right) \\ &- \eta \left(\frac{\partial^4 v}{\partial x^4} + 2 \frac{\partial^4 v}{\partial x^2 \partial y^2} + \frac{\partial^4 v}{\partial y^4} \right) \\ &+ \sigma B_0^2 \sin \beta^* [(u + c) \cos \beta^* - v \sin \beta^*] - \frac{\mu}{k_0} v - \rho g \cos \zeta, \end{aligned} \quad (25)$$

$$\begin{aligned} \rho c_p \left(u \frac{\partial T}{\partial x} + v \frac{\partial T}{\partial y} \right) &= k^* \left(\frac{\partial^2 T}{\partial x^2} + \frac{\partial^2 T}{\partial y^2} \right) \\ &+ \mu \left[2 \left\{ \left(\frac{\partial u}{\partial x} \right)^2 + \left(\frac{\partial v}{\partial y} \right)^2 \right\} + \left(\frac{\partial u}{\partial y} + \frac{\partial v}{\partial x} \right)^2 \right] \\ &+ \eta \left[\left(\frac{\partial^2 u}{\partial x^2} + \frac{\partial^2 u}{\partial y^2} \right)^2 + \left(\frac{\partial^2 v}{\partial x^2} + \frac{\partial^2 v}{\partial y^2} \right)^2 \right] \\ &+ \sigma B_0^2 ((u + c)^2 \cos^2 \beta^* + v^2 \sin^2 \beta^* \\ &- 2(u + c)v \sin \beta^* \cos \beta^*) \\ &+ \frac{16\sigma^* T_0^3}{3\alpha^*} \frac{\partial^2 T}{\partial y^2} + Q_0, \end{aligned} \quad (26)$$

$$\begin{aligned} \left(u \frac{\partial \bar{C}}{\partial x} + v \frac{\partial \bar{C}}{\partial y} \right) &= D \left(\frac{\partial^2 \bar{C}}{\partial x^2} + \frac{\partial^2 \bar{C}}{\partial y^2} \right) \\ &+ \frac{DK_T}{T_m} \left(\frac{\partial^2 T}{\partial x^2} + \frac{\partial^2 T}{\partial y^2} \right) - k_1 \bar{C}. \end{aligned} \quad (27)$$

The appropriate convective boundary conditions are given as follows:

$$\kappa_h \frac{\partial \bar{T}}{\partial y} = -\eta_h (\bar{T} - T_1), \quad \kappa_m \frac{\partial \bar{C}}{\partial y} = -\eta_m (\bar{C} - C_1) \quad \text{at } y = h_1, \quad (28)$$

$$\kappa_h \frac{\partial \bar{T}}{\partial y} = -\eta_h (T_0 - \bar{T}), \quad \kappa_m \frac{\partial \bar{C}}{\partial y} = -\eta_m (C_0 - \bar{C}) \quad \text{at } y = h_2, \quad (29)$$

where κ_h and κ_m are the heat and mass transfer coefficients respectively, η_h and η_m are respective the thermal conductivity and the mass diffusivity coefficients.

The variables are rendered non-dimensional by using the following quantities

$$\begin{aligned} \bar{x} &= \frac{x}{\lambda}, \quad \bar{y} = \frac{y}{d_1}, \quad \bar{u} = \frac{u}{c}, \quad \bar{v} = \frac{v}{c}, \quad h_1 = \frac{H_1}{a_1}, \\ h_2 &= \frac{H_2}{d_1}, \quad \bar{t} = \frac{ct}{\lambda}, \quad \bar{p} = \frac{d_1^2}{\lambda\mu c} p, \quad \delta = \frac{d_1}{\lambda}, \\ d &= \frac{d_2}{d_1}, \quad a = \frac{a_1}{d_1}, \quad b = \frac{a_2}{d_1}, \quad Re = \frac{\rho c d_1}{\mu}, \\ M &= \sqrt{\frac{\sigma}{\mu}} B_0 d_1, \quad Da = \frac{k_0}{d_1^2}, \quad \gamma = \sqrt{\frac{\mu}{\eta}} d_1, \\ Fr &= \frac{c^2}{g d_1}, \quad Ec = \frac{c^2}{c_p(T_1 - T_0)}, \quad \bar{\psi} = \frac{\psi}{c d_1}, \\ Pr &= \frac{\mu c_p}{k^*}, \quad \theta = \frac{\bar{T} - T_0}{T_1 - T_0}, \quad Br = Ec Pr, \\ \varpi &= \frac{Q_0 d_1^2}{k^*(T_1 - T_0)}, \quad \Omega = \frac{\bar{C} - C_0}{C_1 - C_0}, \quad Sc = \frac{\mu}{\rho D}, \\ Sr &= \frac{\rho D K_T (T_1 - T_0)}{\mu T_m (C_1 - C_0)}, \quad Rn = \frac{16\sigma^* T_0^3}{3\alpha^* \mu c_p}, \\ \vartheta &= \frac{\rho k_1 d_1^2}{\mu}, \quad c_1 = \frac{\rho k_1 C_0 d_1^2}{\mu(C_1 - C_0)}, \quad \bar{\beta} = \frac{\beta}{d_1} \quad Bh = \frac{\eta_h d_1}{\kappa_h}, \\ Bm &= \frac{\eta_m d_1}{\kappa_m}, \end{aligned}$$

where δ is the dimensionless wave number, Re is the Reynolds number, M is the Hartmann number, Da is the Darcy number, γ is the couple stress fluid parameter, Pr is the Prandtl number, θ is the dimensionless temperature and ϖ is the heat generation parameter, Br is the Brinkman number, Fr is the Froude number, Ec is the Eckert number, Ω is the dimensionless concentration, Sc is the Schmidt number, Sr is the Soret number, Rn is the thermal radiation parameter, ϑ is the chemical reaction parameter, β is the slip parameter, Bh is the heat transfer Biot number and Bm is the mass transfer Biot number.

Using the above dimensionless parameters in the Eqs. (23)–(27), the governing equations of the fluid flow, after dropping the bars become

$$\delta \frac{\partial u}{\partial x} + \frac{\partial v}{\partial y} = 0, \tag{30}$$

$$\begin{aligned} Re\delta \left(u \frac{\partial u}{\partial x} + \frac{1}{\delta} v \frac{\partial u}{\partial y} \right) &= -\frac{\partial p}{\partial x} + \left(\delta^2 \frac{\partial^2 u}{\partial x^2} + \frac{\partial^2 u}{\partial y^2} \right) \\ &- \frac{1}{\gamma^2} \left(\delta^4 \frac{\partial^4 u}{\partial x^4} + 2\delta^2 \frac{\partial^4 u}{\partial x^2 \partial y^2} + \frac{\partial^4 u}{\partial y^4} \right) \\ &- M^2 \cos \beta^* [(u + 1) \cos \beta^* - v \sin \beta^*] \\ &- \frac{1}{Da} (u + 1) + \frac{Re}{Fr} \sin \zeta, \end{aligned} \tag{31}$$

$$\begin{aligned} Re\delta^2 \left(u \frac{\partial v}{\partial x} + \frac{1}{\delta} v \frac{\partial v}{\partial y} \right) &= -\frac{\partial p}{\partial y} + \left(\delta^3 \frac{\partial^2 v}{\partial x^2} + \delta \frac{\partial^2 v}{\partial y^2} \right) \\ &- \frac{1}{\gamma^2} \left(\delta^5 \frac{\partial^4 v}{\partial x^4} + 2\delta^3 \frac{\partial^4 v}{\partial x^2 \partial y^2} + \delta \frac{\partial^4 v}{\partial y^4} \right) \\ &+ \delta M^2 \sin \beta^* [(u + 1) \cos \beta^* - v \sin \beta^*] \\ &- \frac{1}{Da} \delta v - \delta \frac{Re}{Fr} \cos \zeta, \end{aligned} \tag{32}$$

$$\begin{aligned} RePr\delta \left(u \frac{\partial \theta}{\partial x} + \frac{1}{\delta} v \frac{\partial \theta}{\partial y} \right) &= \left(\delta^2 \frac{\partial^2 \theta}{\partial x^2} + \frac{\partial^2 \theta}{\partial y^2} \right) \\ &+ Br \left[2\delta^2 \left(\frac{\partial u}{\partial x} \right)^2 + 2 \left(\frac{\partial v}{\partial y} \right)^2 + \left(\frac{\partial u}{\partial y} + \delta \frac{\partial v}{\partial x} \right)^2 \right. \\ &+ \frac{1}{\gamma^2} \left\{ \left(\delta^2 \frac{\partial^2 u}{\partial x^2} + \frac{\partial^2 u}{\partial y^2} \right)^2 + \left(\delta^2 \frac{\partial^2 v}{\partial x^2} + \frac{\partial^2 v}{\partial y^2} \right)^2 \right\} \\ &+ M^2 \left\{ (u + 1)^2 \cos^2 \beta^* + v^2 \sin^2 \beta^* - 2(u + 1) \right. \\ &\left. v \sin \beta^* \cos \beta^* \right\} \\ &+ RnPr \frac{\partial^2 \theta}{\partial y^2} + \varpi, \end{aligned} \tag{33}$$

$$\begin{aligned} Re\delta \left(u \frac{\partial \Omega}{\partial x} + \frac{1}{\delta} v \frac{\partial \Omega}{\partial y} \right) &= \frac{1}{Sc} \left(\delta^2 \frac{\partial^2 \Omega}{\partial x^2} + \frac{\partial^2 \Omega}{\partial y^2} \right) \\ &+ Sr \left(\delta^2 \frac{\partial^2 \theta}{\partial x^2} + \frac{\partial^2 \theta}{\partial y^2} \right) - \vartheta \Omega - c_1. \end{aligned} \tag{34}$$

The non-dimensional velocity components (u, v) in terms of stream function ψ are related by the relations $u = \frac{\partial \psi}{\partial y}$ and $v = -\delta \frac{\partial \psi}{\partial x}$. Notice that the equation of continuity (30) is identically satisfied and the governing equations (31)–(34) become

$$\begin{aligned} Re\delta \left[\left(\frac{\partial \psi}{\partial y} \frac{\partial}{\partial x} - \frac{\partial \psi}{\partial x} \frac{\partial}{\partial y} \right) \frac{\partial \psi}{\partial y} \right] &= -\frac{\partial p}{\partial x} + \left(\delta^2 \frac{\partial^3 \psi}{\partial x^2 \partial y} + \frac{\partial^3 \psi}{\partial y^3} \right) \\ &- \frac{1}{\gamma^2} \left(\delta^4 \frac{\partial^5 \psi}{\partial x^4 \partial y} + 2\delta^2 \frac{\partial^5 \psi}{\partial x^2 \partial y^3} + \frac{\partial^5 \psi}{\partial y^5} \right) \\ &- M^2 \cos \beta^* \left[\left(\frac{\partial \psi}{\partial y} + 1 \right) \cos \beta^* + \delta \frac{\partial \psi}{\partial x} \sin \beta^* \right] \\ &- \frac{1}{Da} \left(\frac{\partial \psi}{\partial y} + 1 \right) + \frac{Re}{Fr} \sin \zeta, \end{aligned} \tag{35}$$

$$\begin{aligned}
 Re\delta^3 \left[\left(\frac{\partial\psi}{\partial x} \frac{\partial}{\partial y} - \frac{\partial\psi}{\partial y} \frac{\partial}{\partial x} \right) \frac{\partial\psi}{\partial x} \right] &= -\frac{\partial p}{\partial y} - \left(\delta^4 \frac{\partial^3\psi}{\partial x^3} + \delta^2 \frac{\partial^3\psi}{\partial x\partial y^2} \right) \\
 + \frac{1}{\gamma^2} \left(\delta^6 \frac{\partial^5\psi}{\partial x^5} + 2\delta^4 \frac{\partial^5\psi}{\partial x^3\partial y^2} + \delta^2 \frac{\partial^5\psi}{\partial x\partial y^4} \right) \\
 + \delta M^2 \sin\beta^* \left[\left(\frac{\partial\psi}{\partial y} + 1 \right) \cos\beta^* + \delta \frac{\partial\psi}{\partial x} \sin\beta^* \right] &+ \frac{1}{D_a} \delta^2 \frac{\partial\psi}{\partial x} \\
 - \delta \frac{Re}{Fr} \cos\varsigma, &
 \end{aligned} \tag{36}$$

$$\begin{aligned}
 RePr\delta \left(\frac{\partial\psi}{\partial y} \frac{\partial\theta}{\partial x} - \frac{\partial\psi}{\partial x} \frac{\partial\theta}{\partial y} \right) &= \left(\delta^2 \frac{\partial^2\theta}{\partial x^2} + \frac{\partial^2\theta}{\partial y^2} \right) \\
 + Br \left[4\delta^2 \left(\frac{\partial^2\psi}{\partial x\partial y} \right)^2 + \left(\frac{\partial^2\psi}{\partial y^2} - \delta^2 \frac{\partial^2\psi}{\partial x^2} \right)^2 \right. \\
 + \frac{1}{\gamma^2} \left\{ \left(\delta^2 \frac{\partial^3\psi}{\partial x^2\partial y} + \frac{\partial^3\psi}{\partial y^3} \right)^2 + \left(\delta^3 \frac{\partial^3\psi}{\partial x^3} + \delta \frac{\partial^3\psi}{\partial x\partial y^2} \right)^2 \right\} \\
 + M^2 \left\{ \left(\frac{\partial\psi}{\partial y} + 1 \right)^2 \cos^2\beta^* + \delta^2 \left(\frac{\partial\psi}{\partial y} \right)^2 \sin^2\beta^* \right. \\
 + 2\delta \left(\frac{\partial\psi}{\partial y} + 1 \right) \frac{\partial\psi}{\partial x} \sin\beta^* \cos\beta^* \left. \right\} &+ RnPr \frac{\partial^2\theta}{\partial y^2} + \varpi,
 \end{aligned} \tag{37}$$

$$\begin{aligned}
 Re\delta \left(\frac{\partial\psi}{\partial y} \frac{\partial\Omega}{\partial x} - \frac{\partial\psi}{\partial x} \frac{\partial\Omega}{\partial y} \right) &= \frac{1}{Sc} \left(\delta^2 \frac{\partial^2\Omega}{\partial x^2} + \frac{\partial^2\Omega}{\partial y^2} \right) \\
 + Sr \left(\delta^2 \frac{\partial^2\theta}{\partial x^2} + \frac{\partial^2\theta}{\partial y^2} \right) - \vartheta\Omega - c_1. &
 \end{aligned} \tag{38}$$

The long wavelength ($\delta \approx 0$) and low Reynolds number ($Re \approx 0$) approximations are used throughout our analysis for peristaltic type flows. Such validations remain applicable for the case of chyme transport in small the intestine (Wang et al. 2011). In this case half width is $a = 1.25$ cm and $\lambda = 8.01$ cm. Here half width of the intestine is small compared to the wavelength of peristaltic wave i.e. $a/\lambda = 0.156$. Mustafa et al. (2014) concluded that the Reynolds number for fluid in small intestine is small. Such assumptions also hold good for the human ureter.

Under these assumptions the dimensionless forms of the Eqs. (35)–(38) can be reduced to

$$\begin{aligned}
 \frac{\partial p}{\partial x} &= \frac{\partial^3\psi}{\partial y^3} - \frac{1}{\gamma^2} \frac{\partial^5\psi}{\partial y^5} - \left(M^2 \cos^2\beta^* + \frac{1}{D_a} \right) \left(\frac{\partial\psi}{\partial y} + 1 \right) \\
 + \frac{Re}{Fr} \sin\varsigma, &
 \end{aligned} \tag{39}$$

$$\frac{\partial p}{\partial y} = 0, \tag{40}$$

$$\begin{aligned}
 (1 + RnPr) \frac{\partial^2\theta}{\partial y^2} + Br \left[\left(\frac{\partial^2\psi}{\partial y^2} \right)^2 + \frac{1}{\gamma^2} \left(\frac{\partial^3\psi}{\partial y^3} \right)^2 \right. \\
 + M^2 \cos^2\beta^* \left(\frac{\partial\psi}{\partial y} + 1 \right)^2 \left. \right] + \varpi = 0, &
 \end{aligned} \tag{41}$$

$$\frac{1}{Sc} \frac{\partial^2\Omega}{\partial y^2} + Sr \frac{\partial^2\theta}{\partial y^2} - \vartheta\Omega - c_1 = 0. \tag{42}$$

The dimensionless boundary conditions can be written in the form

$$\begin{aligned}
 \psi = \frac{F}{2}, \quad \frac{\partial^3\psi}{\partial y^3} = 0, \quad \frac{\partial\psi}{\partial y} + \beta \frac{\partial^2\psi}{\partial y^2} = -1, \\
 \frac{\partial\theta}{\partial y} + Bh(\theta - 1) = 0, \quad \frac{\partial\Omega}{\partial y} + Bm(\Omega - 1) = 0 \quad \text{at } y = h_1,
 \end{aligned} \tag{43}$$

$$\begin{aligned}
 \psi = -\frac{F}{2}, \quad \frac{\partial^3\psi}{\partial y^3} = 0, \quad \frac{\partial\psi}{\partial y} - \beta \frac{\partial^2\psi}{\partial y^2} = -1, \\
 \frac{\partial\theta}{\partial y} - Bh\theta = 0, \quad \frac{\partial\Omega}{\partial y} - Bm\Omega = 0 \quad \text{at } y = h_2,
 \end{aligned} \tag{44}$$

in which F is the dimensionless time mean flow rate in the wave frame and it is related to the dimensionless time mean flow rate Θ in the fixed frame by the following expression

$$\Theta = F + 1 + d, \quad F = \int_{h_2}^{h_1} \frac{\partial\psi}{\partial y} dy, \tag{45}$$

where $h_1 = 1 + a \cos(2\pi x)$ and $h_2 = -d - b \cos(2\pi x + \phi)$ represent the dimensionless forms of the surfaces of the peristaltic walls, and a, b, d and ϕ satisfy the relation $a^2 + b^2 + 2ab \cos\phi \leq (1 + d)^2$.

Using Eqs. (39)–(42), with boundary conditions (43)–(44), the exact solutions for the stream function, pressure gradient, temperature and concentration are given as follows:

$$\begin{aligned}
 \psi &= \frac{1}{n_1} (A_1 y + A_2) + A_3 \cosh(m_1 y) + A_4 \sinh(m_1 y) \\
 &+ A_5 \cosh(m_2 y) + A_6 \sinh(m_2 y),
 \end{aligned} \tag{46}$$

$$\frac{\partial p}{\partial x} = \frac{A_1}{\gamma^2} - \left(M^2 \cos^2\beta^* + \frac{1}{D_a} \right) + \frac{Re}{Fr} \sin\varsigma, \tag{47}$$

$$\begin{aligned} \theta = & C_1 \cosh((m_1 + m_2)y) + C_2 \cosh((m_1 - m_2)y) \\ & + C_3 \sinh((m_1 + m_2)y) + C_4 \sinh((m_1 - m_2)y) \\ & + C_5 \cosh(2m_1y) + C_6 \cosh(2m_2y) + C_7 \sinh(2m_1y) \\ & + C_8 \sinh(2m_2y) + C_9 \cosh(m_1y) \\ & + C_{10} \cosh(m_2y) + C_{11} \sinh(m_1y) + C_{12} \sinh(m_2y) \\ & + C_{13}y^2 + C_{14}y + C_{15}, \end{aligned} \tag{48}$$

$$\begin{aligned} \Omega = & D_1 \cosh(m_3y) + D_2 \sinh(m_3y) + D_3 \cosh((m_1 + m_2)y) \\ & + D_4 \cosh((m_1 - m_2)y) \\ & + D_5 \sinh((m_1 + m_2)y) + D_6 \sinh((m_1 - m_2)y) \\ & + D_7 \cosh(2m_1y) + D_8 \cosh(2m_2y) \\ & + D_9 \sinh(2m_1y) + D_{10} \sinh(2m_2y) + D_{11} \cosh(m_1y) \\ & + D_{12} \cosh(m_2y) + D_{13} \sinh(m_1y) \\ & + D_{14} \sinh(m_2y) + D_{15}, \end{aligned} \tag{49}$$

where n_i, m_i 's ($i = 1 - 3$), A_j 's ($j = 1 - 6$), C_l 's ($l = 1 - 15$), and D_f 's ($f = 1 - 15$), can be obtained through simple algebraic computations.

The expression for heat transfer coefficients at the walls h_1 and h_2 are given by

$$Z_{h_1} = \frac{\partial h_1}{\partial x} \frac{\partial \theta}{\partial y} \quad \text{and} \quad Z_{h_2} = \frac{\partial h_2}{\partial x} \frac{\partial \theta}{\partial y}. \tag{50}$$

The expressions for the coefficients of heat transfer from the Eqs. (48) and (50) are

$$\begin{aligned} Z_{h_1} = & -2a\pi \sin(2\pi x)[C_1(m_1 + m_2) \sinh((m_1 + m_2)y) \\ & + C_1(m_1 - m_2) \sinh((m_1 - m_2)y) \\ & + C_3(m_1 + m_2) \cosh((m_1 + m_2)y) \\ & + C_4(m_1 - m_2) \cosh((m_1 - m_2)y) \\ & + 2C_5m_1 \sinh(2m_1y) \\ & + 2C_6m_2 \sinh(2m_2y) + 2C_7m_1 \cosh(2m_1y) \\ & + 2C_8m_2 \cosh(2m_2y) + C_9m_1 \sinh(m_1y) \\ & + C_{10}m_2 \sinh(m_2y) + C_{11}m_1 \cosh(m_1y) \\ & + C_{12}m_2 \cosh(m_2y) + 2C_{13}y + C_{14}], \end{aligned} \tag{51}$$

$$\begin{aligned} Z_{h_2} = & 2b\pi \sin(2\pi x + \phi)[C_1(m_1 + m_2) \sinh((m_1 + m_2)y) \\ & + C_1(m_1 - m_2) \sinh((m_1 - m_2)y) \\ & + C_3(m_1 + m_2) \cosh((m_1 + m_2)y) \\ & + C_4(m_1 - m_2) \cosh((m_1 - m_2)y) \\ & + 2C_5m_1 \sinh(2m_1y) \\ & + 2C_6m_2 \sinh(2m_2y) + 2C_7m_1 \cosh(2m_1y) \\ & + 2C_8m_2 \cosh(2m_2y) + C_9m_1 \sinh(m_1y) \\ & + C_{10}m_2 \sinh(m_2y) + C_{11}m_1 \cosh(m_1y) \\ & + C_{12}m_2 \cosh(m_2y) + 2C_{13}y + C_{14}]. \end{aligned} \tag{52}$$

The dimensionless Nusselt number Nu and Sherwood number Sh at the peristaltic wall $y = h_1$ are obtained by the relations

$$Nu = -\left(\frac{\partial \theta}{\partial y}\right)_{y=h_1}, \quad Sh = -\left(\frac{\partial \Omega}{\partial y}\right)_{y=h_1}. \tag{53}$$

3 Entropy generation analysis

The inherent irreversibility in the channel flow of a couple stress fluid arises due to the exchange of energy and momentum, within the fluid and at solid boundaries. Accordingly, the entropy production may occur as a result of fluid friction, radiation, heat generation and heat transfer in the direction of finite temperature gradients. The entropy generation can be defined in the wave frame as follows Akbar (2015)

$$\begin{aligned} S_G = & \frac{k^*}{T_0^2} \left(\left(\frac{\partial \bar{T}}{\partial x}\right)^2 + \left(\frac{\partial \bar{T}}{\partial y}\right)^2 + \frac{16\sigma^* T_0^2}{3\alpha^* k^*} \left(\frac{\partial \bar{T}}{\partial y}\right)^2 \right) \\ & + \frac{\mu}{T_0} \left[2 \left\{ \left(\frac{\partial u}{\partial x}\right)^2 + \left(\frac{\partial v}{\partial y}\right)^2 \right\} + \left(\frac{\partial u}{\partial y} + \frac{\partial v}{\partial x}\right)^2 \right] \\ & + \frac{\eta}{T_0} \left[\left(\frac{\partial^2 u}{\partial x^2} + \frac{\partial^2 u}{\partial y^2}\right)^2 + \left(\frac{\partial^2 v}{\partial x^2} + \frac{\partial^2 v}{\partial y^2}\right)^2 \right] \\ & + \frac{\sigma B_0^2}{T_0} ((u + c)^2 \cos^2 \beta^* + v^2 \sin^2 \beta^* \\ & - 2(u + c)v \sin \beta^* \cos \beta^*) + \frac{Q_0}{T_0}. \end{aligned} \tag{54}$$

The non-dimensional form of entropy generation, using the relations of stream functions and long wavelength assumption, can be reduced to

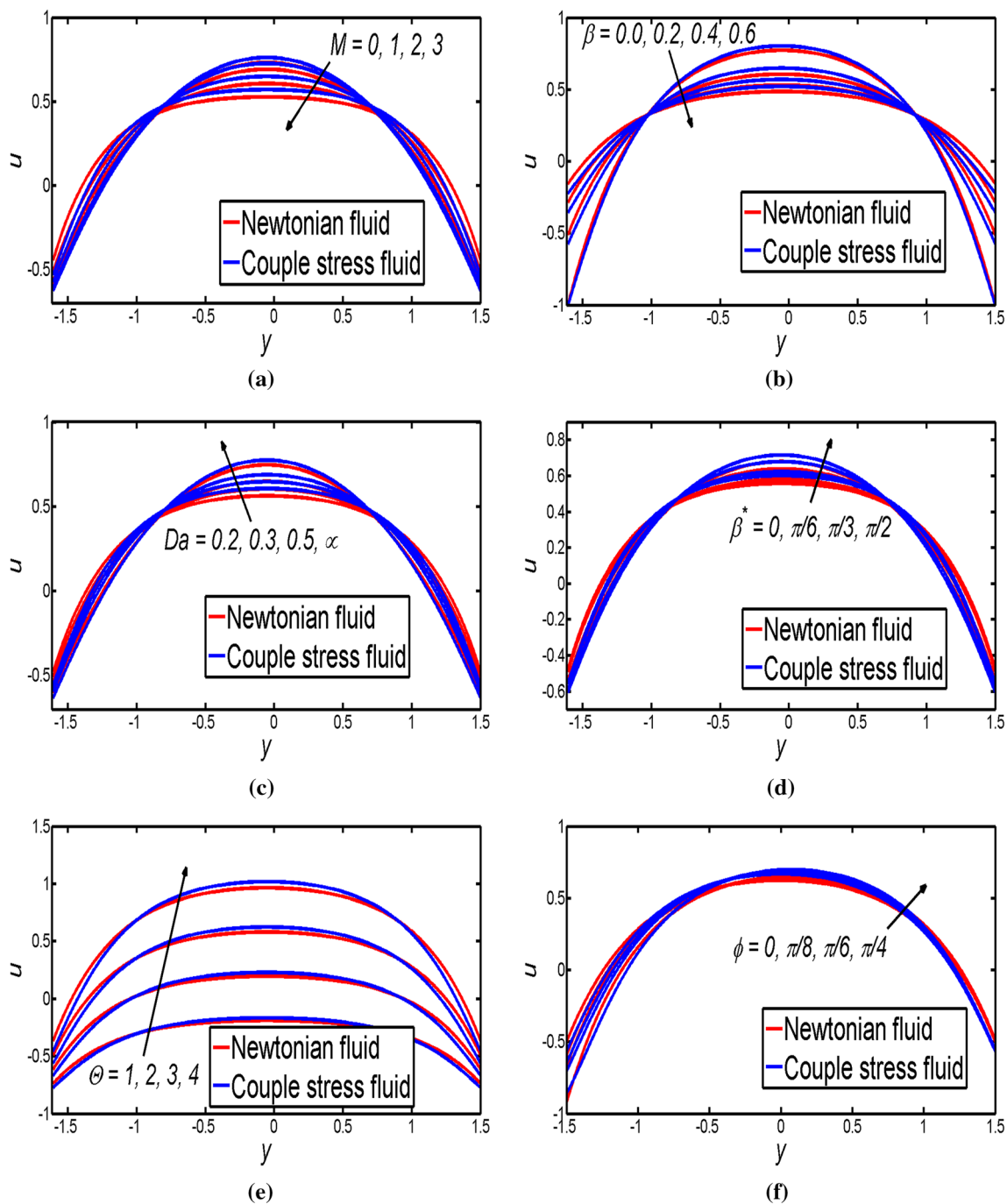


Fig. 1 Effect of different fluid parameters on the velocity profiles

$$\begin{aligned}
 Ns = & (1 + RnPr) \left(\frac{\partial \theta}{\partial y} \right)^2 + \frac{Br}{\Lambda} \left(\left(\frac{\partial^2 \psi}{\partial y^2} \right)^2 + \frac{1}{\gamma^2} \left(\frac{\partial^3 \psi}{\partial y^3} \right)^2 \right) \\
 & + \frac{BrM^2 \cos^2 \beta^*}{\Lambda} \left(\frac{\partial \psi}{\partial y} + 1 \right)^2 + \frac{\varpi}{\Lambda},
 \end{aligned}
 \tag{55}$$

where $\Lambda = (T_1 - T_0)/T_0$ is the temperature difference parameter, $Ns = S_G/S_{G_0}$, in which, S_G is the dimensionless

form of entropy generation number, $S_{G_0} = k^*(T_1 - T_0)^2/T_0^2 d_1^2$ is the volumetric entropy generation and Ns is the ratio of actual entropy generation rate to the reference volumetric entropy generation. The total entropy generation in the equation (55) can be written as the sum

$$Ns = N_H + (N_V + N_M + N_G) = N_H + N_B,
 \tag{56}$$

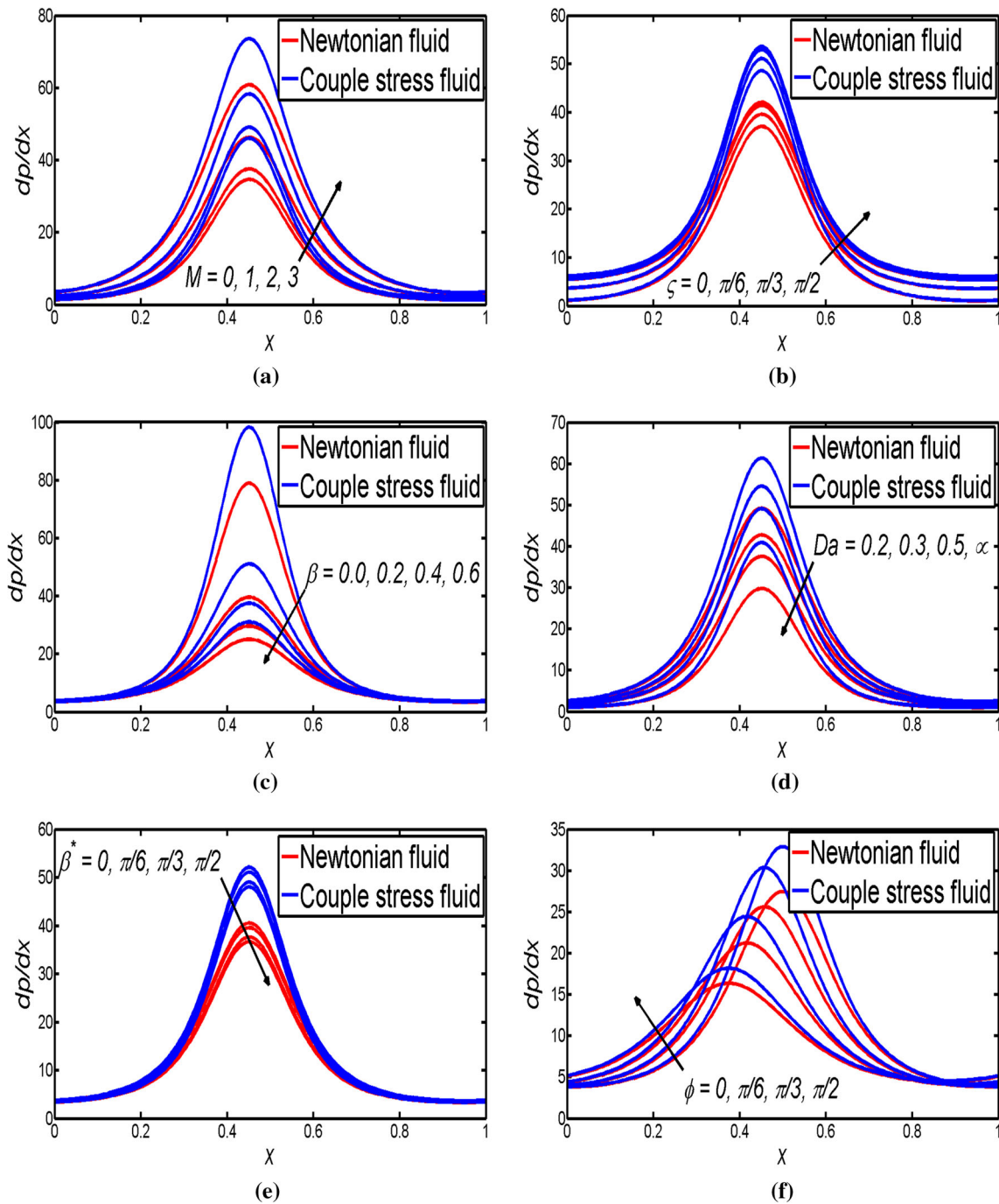


Fig. 2 Effect of different fluid parameters on the pressure gradient profiles

where N_H denotes the entropy generation due to heat transfer, N_V is the entropy generation due to fluid friction, N_M is the entropy generation due to magnetic field, and N_G entropy generation due to heat generation. Further, N_B can be treated as the entropy generation due to combined effects of fluid friction, magnetic field and heat generation.

The Bejan number Be is a parameter that measures the irreversibility ratio in the heat flow defined as

$$Be = \frac{N_H}{N_s} = \frac{1}{1 + \xi}, \quad \xi = \frac{N_B}{N_H}, \tag{57}$$

where parameter ξ is the irreversibility ratio that measures the rate of destruction of available work in the flow system. The Bejan number is bounded in the interval $0 \leq Be \leq 1$. The irreversibility due to heat transfer is dominant when $Be = 1$, while the irreversibility due to fluid friction, heat generation and magnetic field is dominant when $Be = 0$

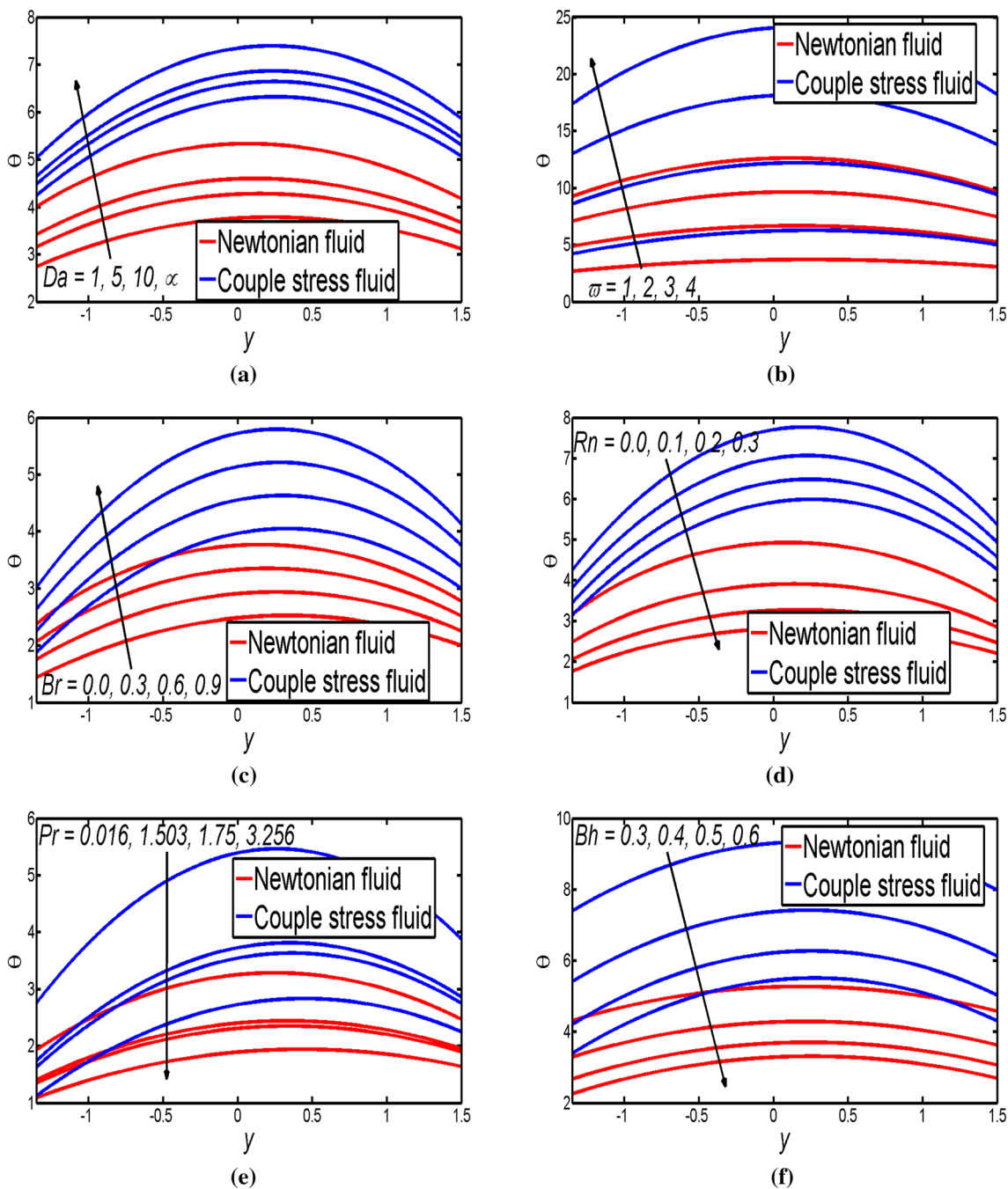


Fig. 3 Effect of different fluid parameters on the temperature profiles

and $Be = 0.5$ is the case where the contributions of both heat and fluid friction to entropy generation are equal.

4 Results and discussion

This segment is devoted to study the physical impact of important quantities velocity u , pressure gradient dp/dx , temperature θ , heat transfer coefficient Z_{h1} , concentration

Ω , entropy generation N_s and Bejan number Be graphically. The behavior of different wave forms is also discussed in the form of streamlines. The results of Nusselt number Nu are presented in terms of tabular forms. A comparison for the Newtonian fluid model and couple stress fluid model is also presented. In all the situations the same behavior is observed for Newtonian fluid and couple stress fluid models.

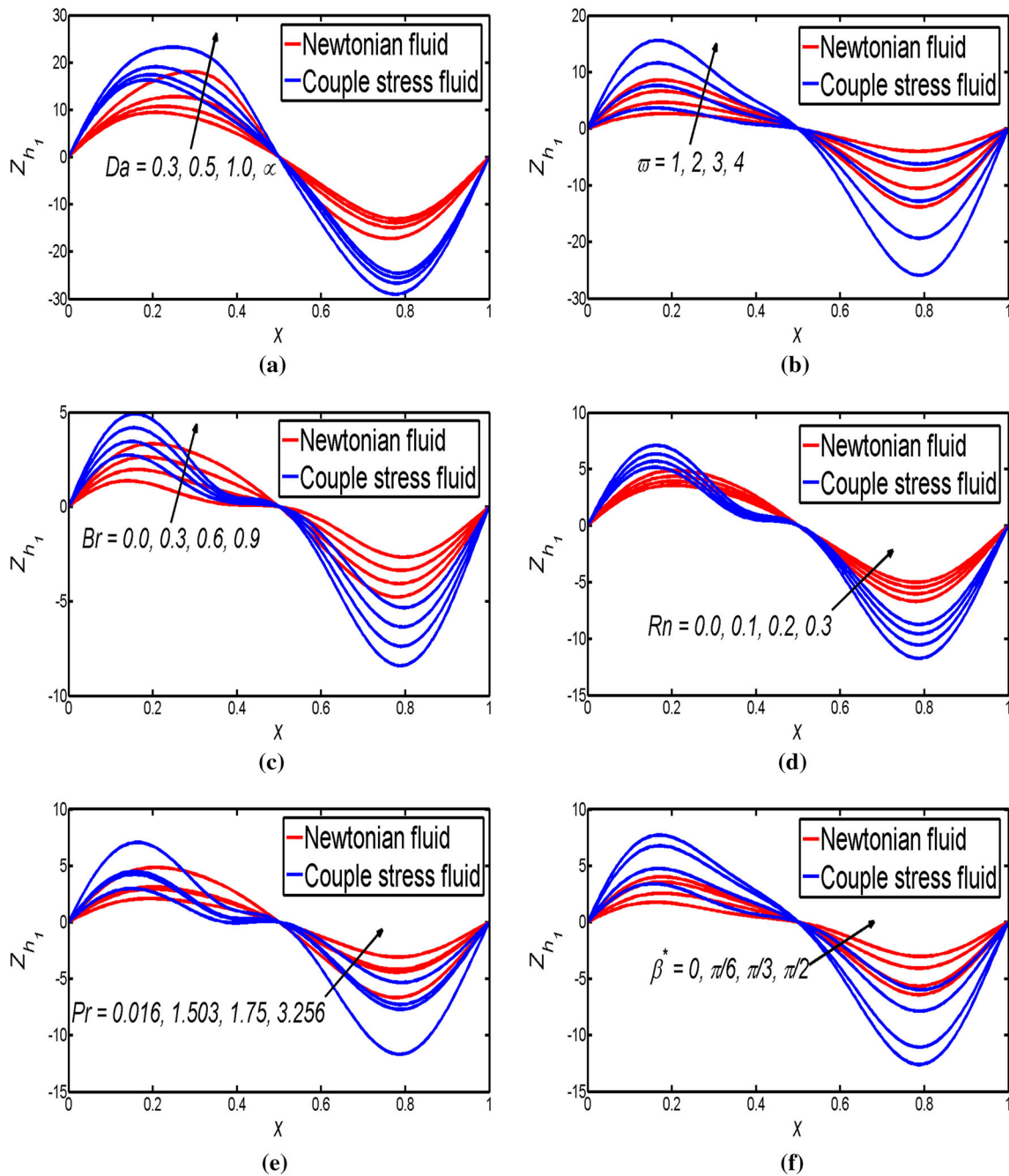


Fig. 4 Effect of different fluid parameters on the heat transfer coefficients

4.1 Velocity characteristics

Figure 1 is prepared to analyze the impacts of Hartmann number M , slip parameter β , Darcy number Da , inclination angle of magnetic field β^* , volume flow rate Θ and phase difference ϕ on the axial velocity. It is observed from Fig. 1 that, the velocity profile traces a parabolic trajectory with maximum value occurring near the center of the channel. It is also observed that, the higher velocity profiles can be seen in couple stress fluid model as compared to the

Newtonian fluid model near the center of the channel. Figure 1a shows that, the velocity profile decreases near the center of the channel and increases near the boundaries with increase of Hartmann number. This is for the reason that, the application of the transverse magnetic field plays the role of a resistive type force (Lorentz force) similar to drag force (that acts in the opposite direction of the fluid motion), which tends to resist the flow thereby reducing its velocity. This result is in good agreement with the references (Akbar 2015; Ramesh 2016). It is noted from Fig. 1b

Table 1 Variation of Nusselt number for various values of heat generation parameter

x	ϖ			
	1	2	3	4
0.0	0.5991	1.4134	2.2276	3.0419
0.1	0.4284	1.0945	1.7606	2.4267
0.2	0.2088	0.6906	1.1723	1.6540
0.3	0.0053	0.3369	0.6686	1.0002

Table 2 Variation of Nusselt number for various values of Hartmann number

x	M			
	0	1	2	3
0.0	1.6605	1.8043	2.1862	2.7507
0.1	1.2826	1.4171	1.7588	2.2421
0.2	0.7837	0.9172	1.2258	1.6172
0.3	0.3080	0.4687	0.7927	1.1322

Table 3 Variation of Nusselt number for various values of thermal radiation parameter

x	Rn			
	0.0	0.1	0.2	0.3
0.0	3.9280	3.5350	3.2076	2.9305
0.1	3.2325	2.8988	2.6206	2.3852
0.2	2.2610	2.0089	1.7989	1.6211
0.3	1.1872	1.0255	0.8908	0.7768

Table 4 Variation of Nusselt number for various values of velocity slip parameter

x	β			
	0.0	0.2	0.4	0.6
0.0	2.0839	1.8977	1.8252	1.7889
0.1	1.7413	1.5182	1.4390	1.4011
0.2	1.2690	1.0137	0.9372	0.9030
0.3	0.4991	0.4888	0.4740	0.4643

that, the velocity increases near the boundary of the peristaltic walls and decreases near the center of the channel with increase of slip parameter. It is physically justified because, when the slip occurs at the boundary, the velocity of the fluid near the boundary is no longer equal to that of

the boundary, and the more the fluid slips at the boundary, the less its velocity is affected by the motion of the boundary. The velocity increases near the center of the channel and decreases near the peristaltic walls with increase of Darcy number (see Fig. 1c). This result gives that, the velocity increases from porous medium to clear medium near the center of the channel. This observation is physically realistic by the fact that, a more permeable porous medium will provide less resistance to the fluid flow and consequently there is an increase in the velocity of fluid. The similar behavior can be seen with increase of inclination angle of magnetic field (see Fig. 1d). It is depicted from Fig. 1e that, the velocity is an increasing function of volume flow rate. It is observed from Fig. 1f that, the velocity decreases near the lower wall and the trend is reversed near the upper wall with increase of phase difference.

4.2 Pumping characteristics

Figure 2 is sketched to analyze the impacts of Hartmann number M , inclination angle of the channel ζ , slip parameter β , Darcy number Da , inclination angle of magnetic field β^* and phase difference ϕ on the pressure gradient. It is observed from the figure that, more pressure gradient is required for couple stress fluid as compared to the Newtonian fluid to maintain the given volume flow rate. It is also noticed from this figure that, in the wider part of the channel $x \in [0, 0.2]$ and $x \in [0.7, 1]$, the pressure gradient is small, so the flow can be easily passed without the imposition of large pressure gradient. However, in the narrow part of the channel $x \in [0.2, 0.7]$, the pressure gradient is large, that is, a much larger pressure gradient is needed to maintain the same given volume flow rate. This is in good agreement with the physical situation. It is noted from Fig. 2a that, the pressure gradient increases with increasing values of Hartmann number. It clearly shows that, when the strong magnetic field is applied to the flow field then higher pressure gradient is needed to pass the flow in the channel. This outcome suggests that, fluid pressure can be controlled by the application of suitable magnetic field strength. This phenomenon is useful during surgery and critical operation to control excessive bleeding. The similar behavior is observed in Akbar (2015). The similar trend is seen with increase of inclination angle of the channel (see Fig. 2b). It is also noticed that, the pressure gradient increases from horizontal channel to vertical channel. It is depicted from Fig. 2c that, the pressure gradient is a decreasing function of Darcy number, this implies that, the larger pressure gradient is required to push the fluid in the presence porous medium as compared to the clear medium. It is well agreement to the physical situation. In the absence of slip

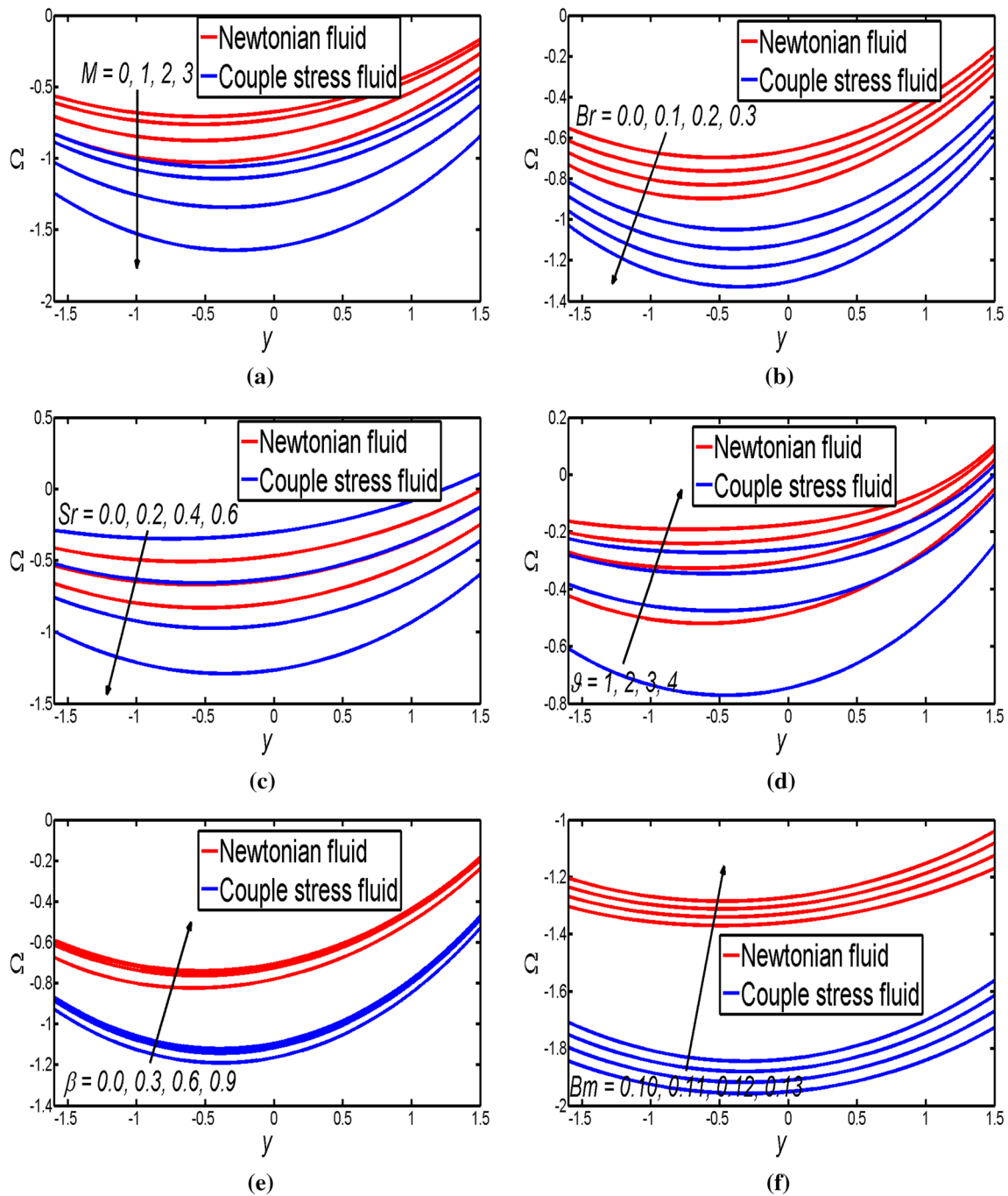


Fig. 5 Effect of different fluid parameters on the concentration profiles

velocity a larger pressure gradient is required in the wider and narrow part of the channel to maintain the given volume flow, the trend is reversed in the presence of slip effects (see Fig. 2d). It is clear from Fig. 2e that, the pressure gradient is an increasing function of inclination angle of the magnetic field. It is observed from Fig. 2f that, with an increase of phase difference, the pressure gradient decreases in the narrow part of the channel and increases in

the wider part of the channel. Moreover, the narrow region is shifted to the left side with an increase in phase difference and a lesser amount of pressure gradient is required to pass the flow in the wider part of an asymmetric channel compared to the symmetric channel. However, it is quite opposite in the wider part of the channel.

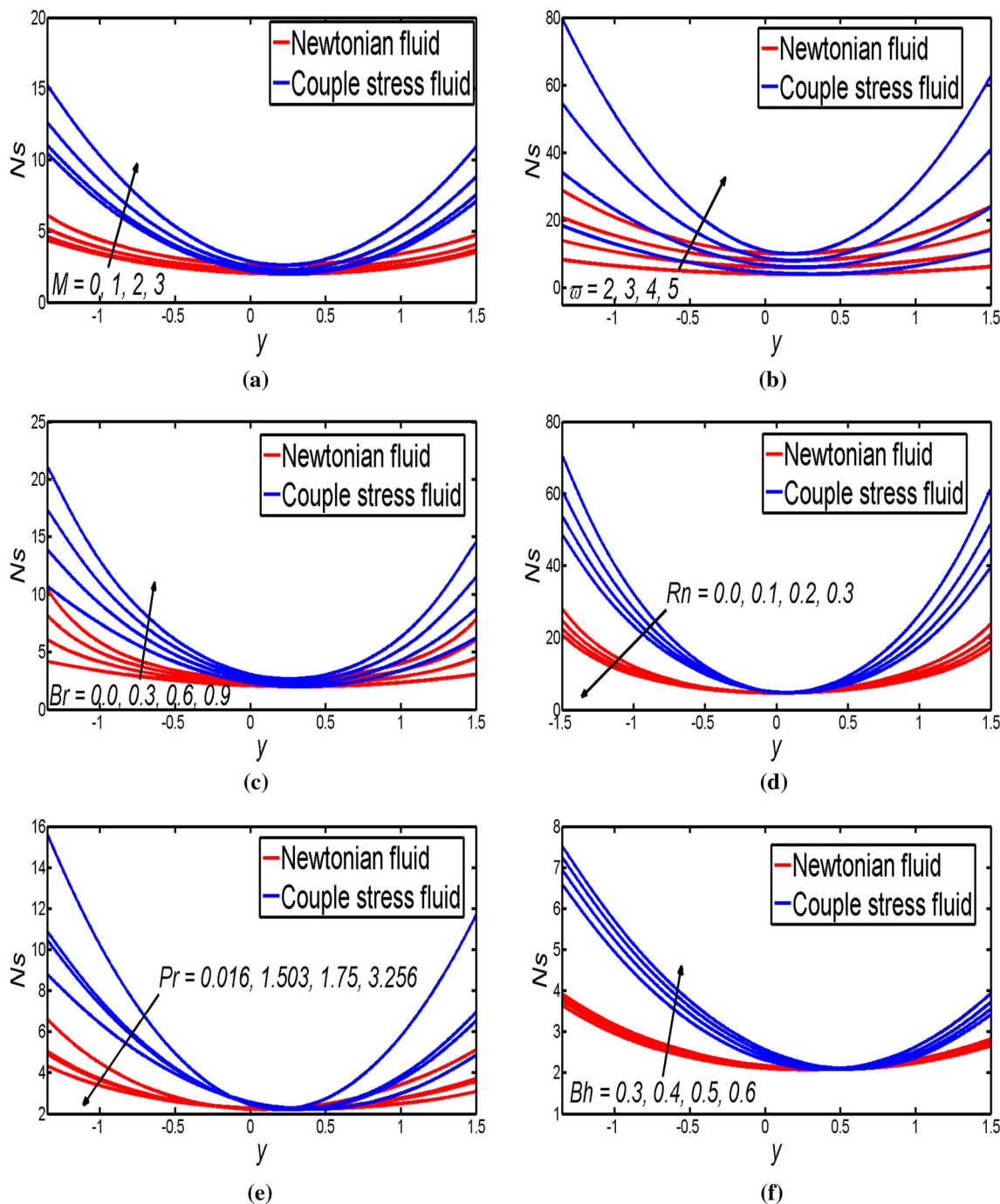


Fig. 6 Effect of different fluid parameters on the entropy generation profiles

4.3 Heat and mass characteristics

Variations in the temperature distribution have been designed in Fig. 3 for different values of Darcy number Da , heat generation parameter ω , Brinkman number Br , thermal radiation parameter Rn , Prandtl number Pr and heat transfer Biot number Bh . It is observed from this figure that, the temperature profiles are almost parabolic in

nature and the higher temperature is seen near the center of the channel. It is also noticed that, in all the situations, the temperature is high for the couple stress fluid model and low for the Newtonian fluid model. It is depicted from Fig. 3a that, the temperature of the fluid is an increasing function of Darcy number. This result due to the porous medium of the channel which disturbs the fluid velocity. As a result the temperature of fluid is raised. This shows that,

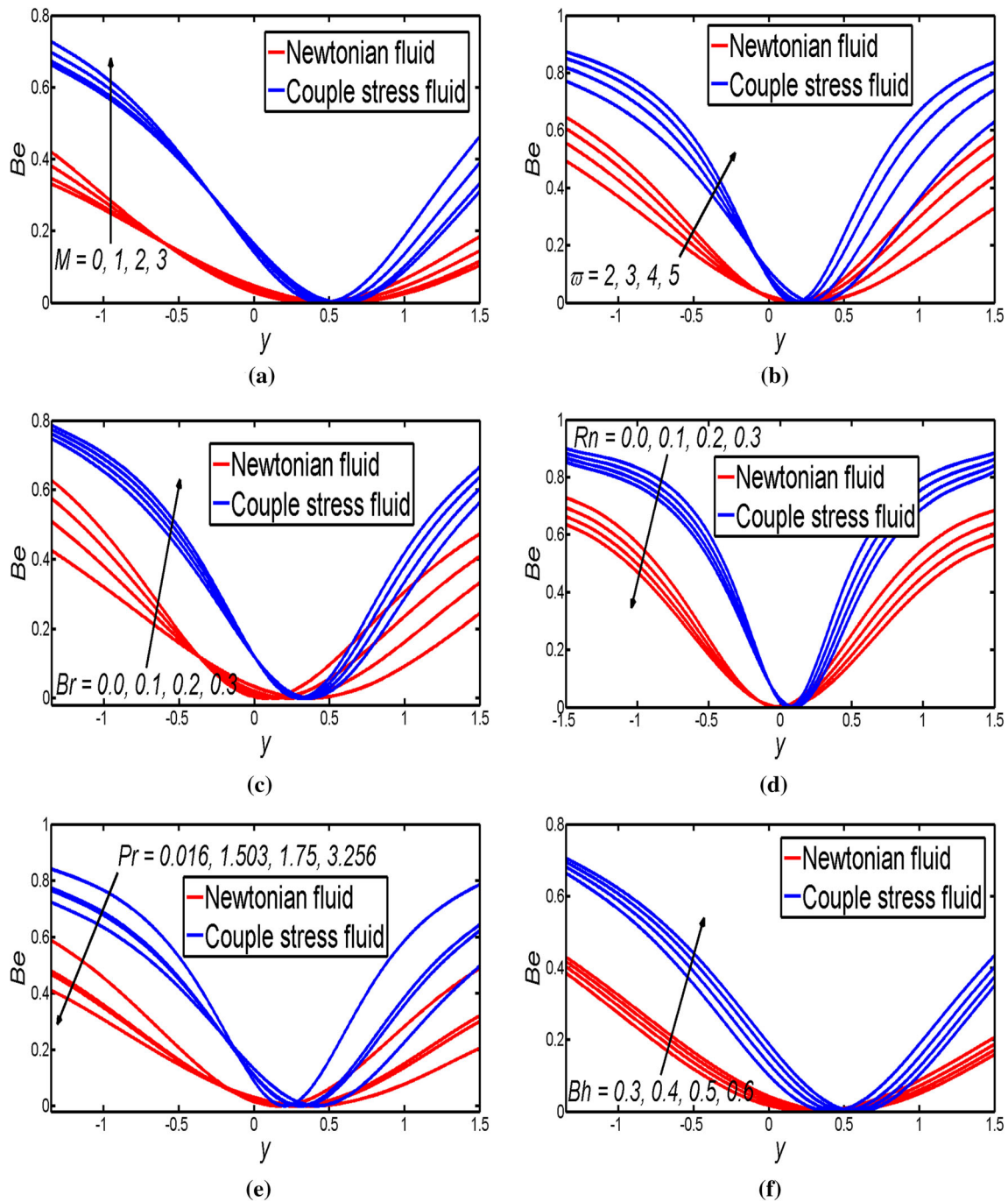


Fig. 7 Effect of different fluid parameters on the Bejan numbers

the higher temperature can be seen in clear medium and lower temperature is seen in porous medium. The temperature increases with increase of heat generation parameter (see Fig. 3b). It is noted from Fig. 3c that, the temperature increases with increase of Brinkman number. It is due to the fact that, an increase in the values of Brinkman number rises the resistance offered by shear in flow which in turn increases the heat generation due to the viscous dissipation effects and hence the temperature of the

fluid increases. It is noticed from Fig. 3d that, for larger values of radiation parameter the temperature decreases. It is in fact due to the loss of heat. The temperature profile is shown in Fig. 3e for different Prandtl numbers of mercury, saturated ammonia, saturated water and isobutane. It is observed from this figure that, the temperature increases with an increase in Prandtl number. Moreover, the higher temperature is seen in isobutane, whereas the lower temperature occurs in mercury. It can be seen from Fig. 3f that,

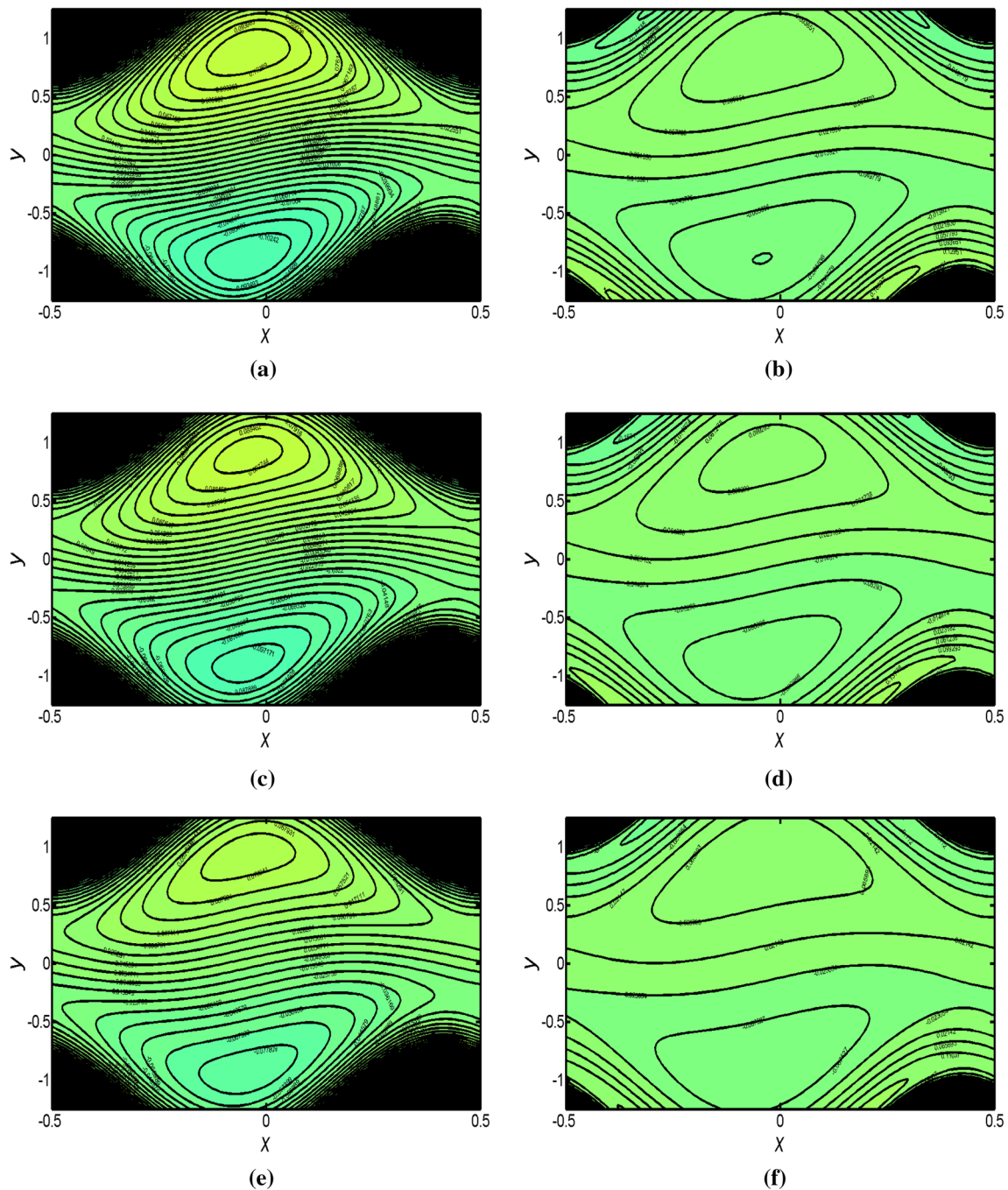


Fig. 8 Streamlines for Newtonian fluid (left panel) and couple stress fluid (right panel) models for various values of Hartmann number

the temperature is a decreasing function of Biot number. It is due to increasing of Biot number reduces the thermal conductivity which causes reduction of the temperature profile. The impression of heat transfer coefficient at the upper wall under the effect of peristalsis is illustrated in Fig. 5. It is depicted from this figure that, heat transfer coefficient is oscillatory. This is due to propagation of sinusoidal waves along the channel walls. It is observed from Fig. 4a–c that, the heat transfer coefficient increases

in magnitude with an increase of Darcy number, heat generation parameter and Brinkman number. The opposite behavior is observed with increase of thermal radiation, Prandtl number and inclination angle of magnetic field (see Fig. 4d–f). The variations of Nusselt number with different parameters can be observed through the Tables 1, 2, 3 and 4. It is depicted from these tables that, Nusselt number is an increasing function of heat generation parameter and Hartmann number. The trend is reversed with increase of

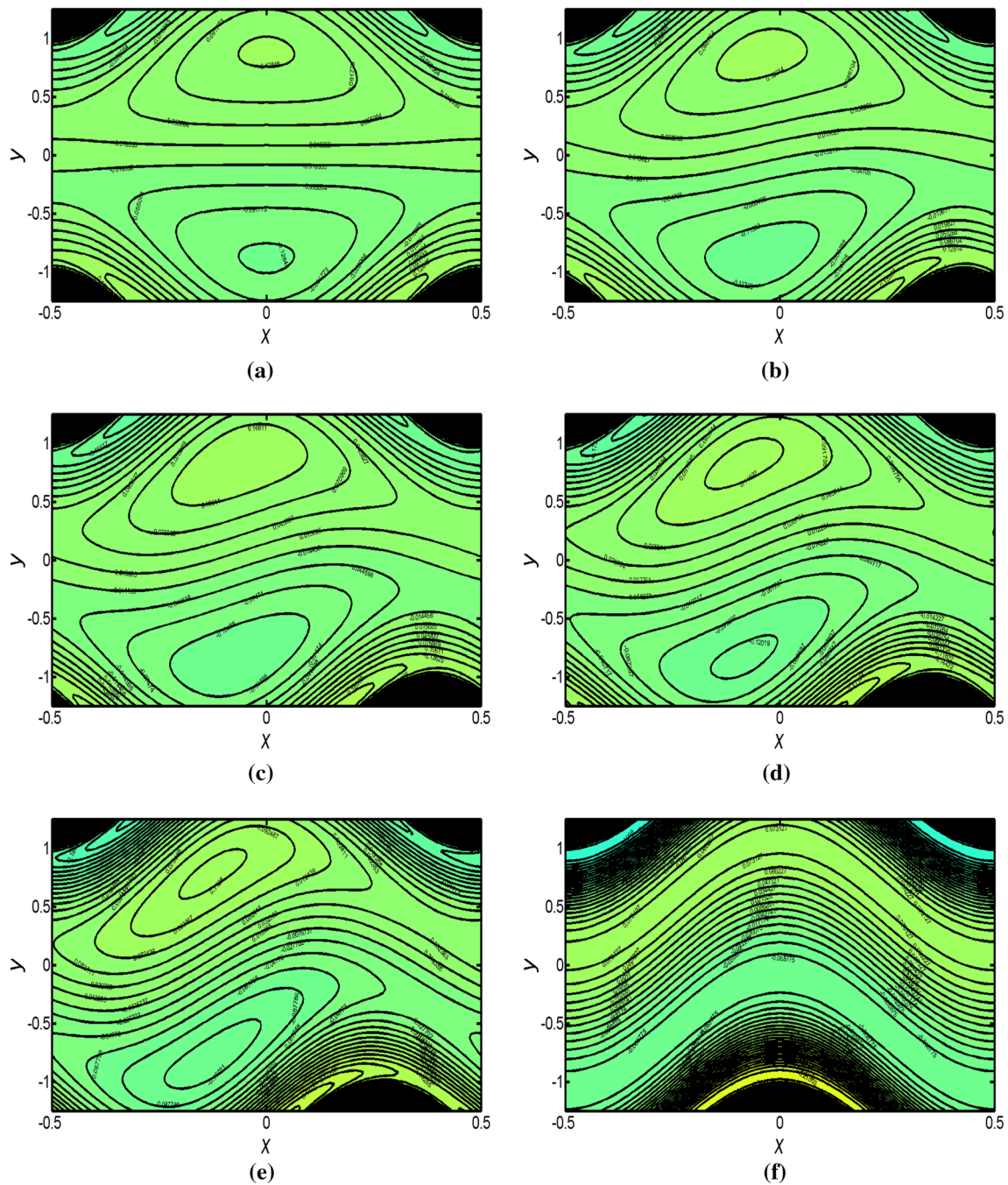


Fig. 9 Streamline patterns for different values of phase difference

thermal radiation and slip parameter. The effect of the dimensionless parameters such as, Hartmann number M , Brinkman number Br , Soret number Sr , chemical reaction parameter ϑ , velocity slip parameter β and mass transfer Biot number Bm on concentration is depicted in Fig. 5. It is observed from this figure that, higher concentration is observed in magnitude for the couple stress fluid model as compared to the Newtonian fluid model. It is depicted from Fig. 5a–c that, the concentration decreases with increase of

Hartmann number, Brinkman number and Soret number. The trend is reversed with increase of chemical reaction parameter, velocity slip parameter and mass transfer Biot number (see Fig. 5d–f).

4.4 Entropy generation

Figure 6 is prepared to analyze the entropy generation N_s with respect to change in different physical constraints

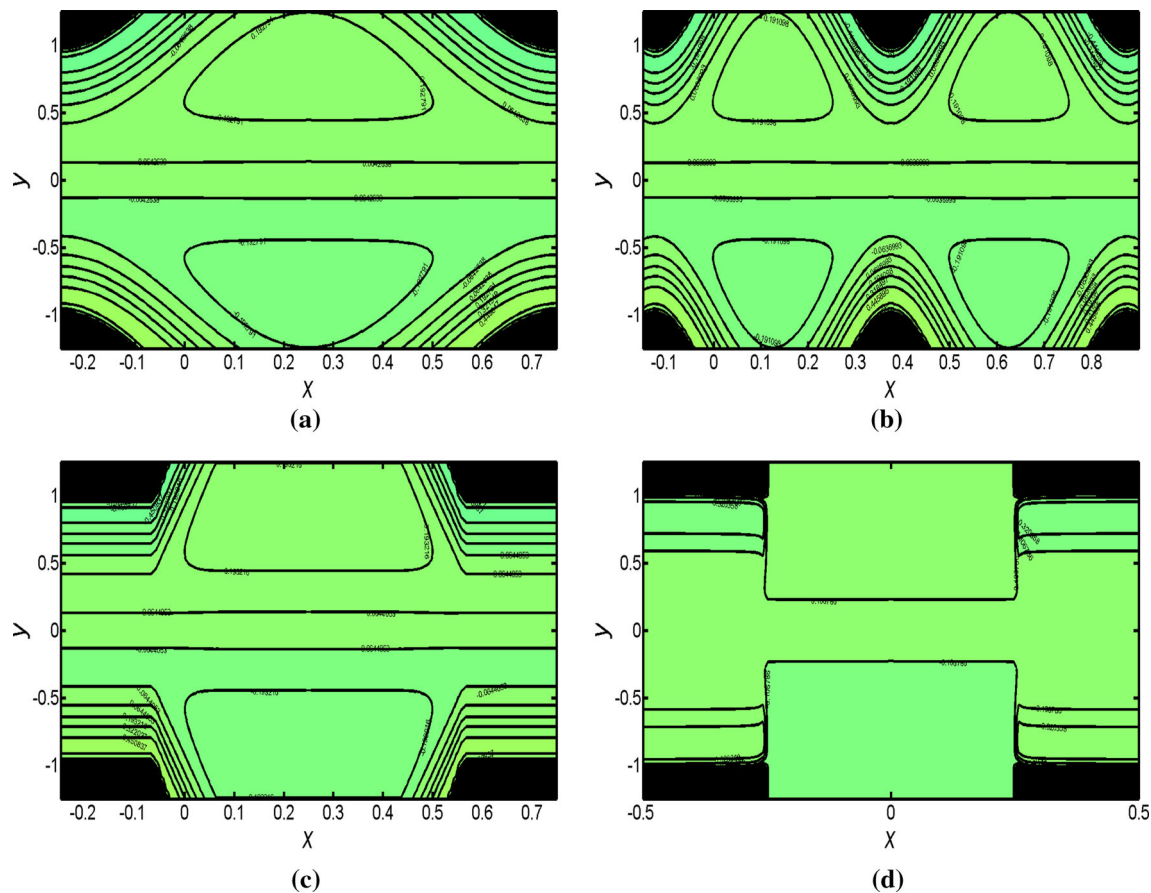


Fig. 10 Streamline profiles for various wave forms with no-slip condition

such as Hartmann number M , heat generation parameter ϖ , Brinkman number Br , thermal radiation parameter Rn , Prandtl number Pr and thermal Biot number Bh . It is observed from this figure that, the higher entropy generation can be seen in the couple stress fluid model and the lower entropy generation is observed in Newtonian fluid model. It is also notes that, It has larger values near the walls of the channel as compared to the center of the channel. It is seen from Fig. 6a–c that, the entropy generation enhances with increase of Hartmann number, heat generation parameter and Brinkman number. Entropy generation reduces when thermal radiation and Prandtl number are enhanced (see Fig. 6d, e). It is depicted from Fig. 6f that, entropy generation increases near the lower wall and decreases near the upper wall with increase of thermal Biot number. Figure 7 is sketched to analyze the Bejan number with respect to change in different physical constraints involved. Figures 7a–c depict that, with increase of Hartmann number, heat generation parameter and Brinkman number, heat transfer irreversibility is high as compared to the total irreversibility due to heat transfer, fluid friction, heat generation and magnetic field near the channel walls. The opposite trend is observed at near the

center of the channel. The opposite behavior is observed with increase of thermal radiation and Prandtl number (see Fig. 7d, e). It is observed from Fig. 7f that, the Bejan number increases near the lower wall and decreases near the upper wall with increase of thermal Biot number.

4.5 Trapping phenomenon

The trapping phenomenon may be looked upon as the formation of an internally circulating bolus in the moving fluid. This trapped bolus is completely enclosed by peristaltic wave and hence moves ahead along with wave at same velocity. The concept of trapping phenomenon on the peristaltic pumping of a fluid was introduced by Shapiro et al. (1969). The trapping phenomenon is prepared in Fig. 8 for various values of Hartmann number for Newtonian fluid and couple stress fluid models. In this figure, the left panels (a), (c) and (e) belong to the Newtonian fluid model and the right panels (b), (d) and (f) correspond to couple stress fluid model. It is observed from this figure that, when Hartmann number increases, the size of the trapped bolus decreases in both fluid models. It is also found that, the number of closed streamlines are greater in

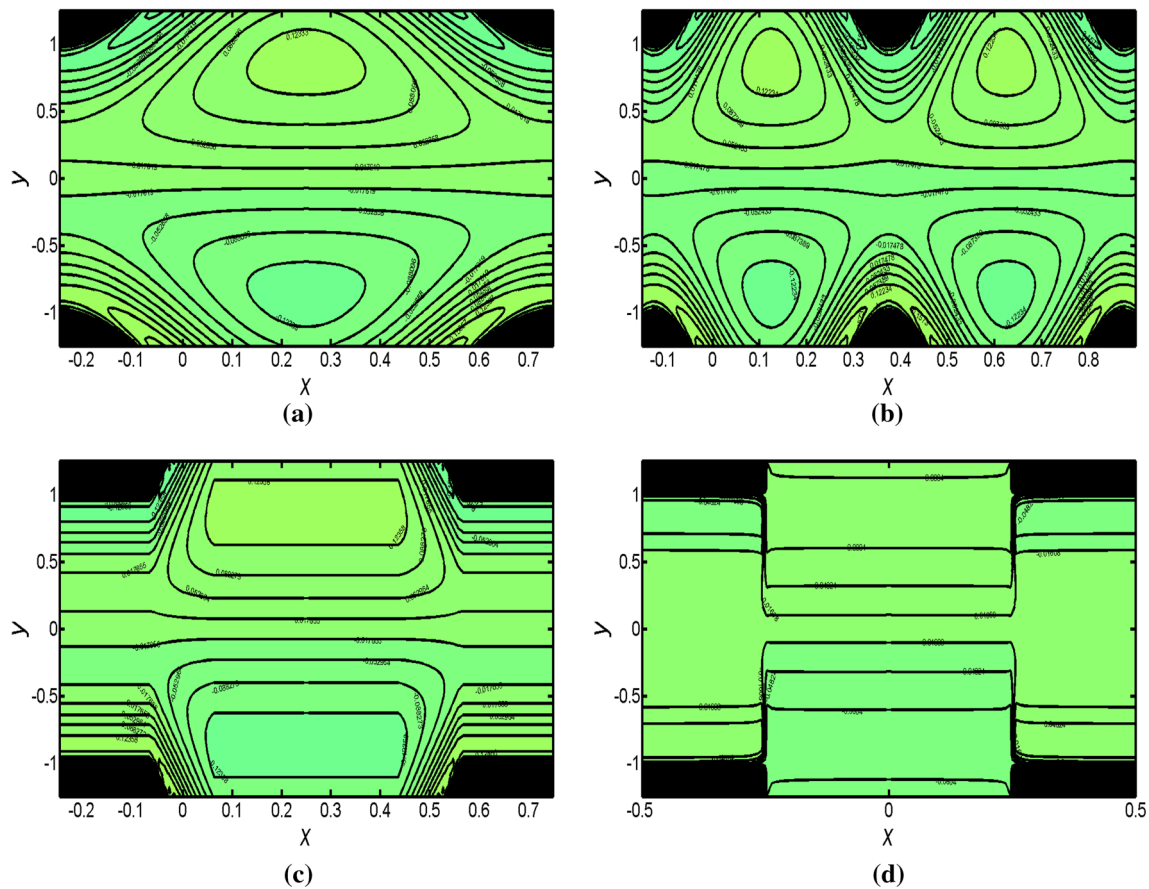


Fig. 11 Streamline profiles for various wave forms with slip condition

the Newtonian fluid model as compared with couple stress fluid model. Figure 9 is sketched to see the behavior of trapping phenomenon for various values of phase difference. It is evident that, as phase difference increases, the trapping bolus decreases and when it reaches to π , the trapping disappears. Moreover, with increase of phase difference, the bolus moves forward with decreasing effect. It is also observed that, the size of trapping bolus is high in the symmetric channel and low for asymmetric channel. Latham (1966) in his experiments, he has given a detailed information about the different wave shapes because of various applications in physiology and industry. In view of this, we have considered six different wave forms namely sinusoidal wave, multi sinusoidal wave, trapezoidal wave and square wave. Figures 10 and 11 provide the variations of slip parameter on the trapping phenomenon for different wave shapes. It is observed from these figures that, the size of the trapped bolus increases with increase of slip parameter in all the wave forms.

5 Conclusions

In the present paper, we have examined the effects of entropy generation and thermal radiation on the peristaltic transport of incompressible couple stress fluid in an inclined asymmetric channel through homogeneous porous medium. The effects of inclined magnetic field, Joule heating, chemical reactions, slip and convective conditions are also taken into account. The governing differential equations for momentum, energy, entropy generation and concentration are modeled and simplified under the long wavelength and low Reynolds number approximations. The exact solutions are presented for stream function, pressure gradient, temperature and concentration. The pertinent parameters appear in the problem have discussed through graphs and tabular forms. Comparison study is made for both Newtonian and couple stress fluid models. The main findings are observed in the present study as follows:

- Velocity of the fluid increases with increase of Hartmann number and slip parameter near the channel walls while velocity decreases near the center of the channel.

- Pressure gradient is an increasing function of Hartmann number and inclination angle of the channel, and the trend is reversed with increase of slip parameter, Darcy number and inclination angle of magnetic field.
- Temperature is a decreasing function of radiation parameter, Prandtl number and thermal Biot number.
- Heat transfer coefficient increases in magnitude with an increase of Darcy number, heat generation parameter and Brinkman number.
- Concentration is an increasing function of chemical reaction parameter, velocity slip parameter and mass transfer Biot number.
- Concentration profiles show the opposite behavior as compared with temperature profiles.
- Entropy generation reduces when thermal radiation and Prandtl number are increased.
- The size of trapping bolus decreases with increase of Hartmann number.
- The size of trapped bolus increases with an increase of slip parameter in all the mentioned wave forms.

References

- Abd elmaboud Y, Mekheimer KS (2011) Non-linear peristaltic transport of a second-order fluid through a porous medium. *Appl Math Model* 35(6):2695–2710
- Abd-Alla AM, Abo-Dahab SM (2015) Magnetic field and rotation effects on peristaltic transport of a Jeffrey fluid in an asymmetric channel. *J Magn Magn Mater* 374:680–689
- Adesanya SO, Kareem SO, Falade JA, Arekete SA (2015) Entropy generation analysis for a reactive couple stress fluid flow through a channel saturated with porous material. *Energy* 93:1239–1245
- Akbar NS (2015) Influence of magnetic field on peristaltic flow of a Casson fluid in an asymmetric channel: application in crude oil refinement. *J Magn Magn Mater* 378:463–468
- Akbar NS (2015) Entropy generation and energy conversion rate for the peristaltic flow in a tube with magnetic field. *Energy* 82:23–30
- Akbar NS, Nadeem S (2011) Simulation of heat transfer on the peristaltic flow of a Jeffrey-six constant fluid in a diverging tube. *Int Commun Heat Mass Transf* 38(2):154–159
- Akbar NS, Nadeem S (2012) Thermal and velocity slip effects on the peristaltic flow of a six constant Jeffrey's fluid model. *Int J Heat Mass Transf* 55(15):3964–3970
- Akbarzadeh M, Rashidi S, Bovand M, Ellahi R (2016) A sensitivity analysis on thermal and pumping power for the flow of nanofluid inside a wavy channel. *J Mol Liquids* 220:1–13
- Akram S, Nadeem S (2013) Influence of induced magnetic field and heat transfer on the peristaltic motion of a Jeffrey fluid in an asymmetric channel: closed form solutions. *J Magn Magn Mater* 328:11–20
- Ali N, Hayat T (2008) Peristaltic flow of a micropolar fluid in an asymmetric channel. *Comput Math Appl* 55(4):589–608
- Anggiansah A, Taylor G, Bright N, Wang J, Owen WA, Rokkas T, Jones AR, Owen WJ (1994) Primary peristalsis is the major acid clearance mechanism in reflux patients. *Gut* 35(11):1536–1542
- Basak T, Anandalakshmi R, Kumar P, Roy S (2012) Entropy generation vs. energy flow due to natural convection in a trapezoidal cavity with isothermal and non-isothermal hot bottom wall. *Energy* 37(1):514–532
- Bejan A (1980) Second law analysis in heat transfer. *Energy* 5:720–732
- Bejan A (2001) Thermodynamic optimization of geometry in engineering flow systems. *Exergy* 4:269–277
- Bhatti MM, Abbas MA (2016) Simultaneous effects of slip and MHD on peristaltic blood flow of Jeffrey fluid model through a porous medium. *Alex Eng J* 55(2):1017–1023
- Bhatti MM, Ellahi R, Zeeshan A (2016) Study of variable magnetic field on the peristaltic flow of Jeffrey fluid in a non-uniform rectangular duct having compliant walls. *J Mol Liquids* 222:101–108
- Bhatti MM, Zeeshan A, Ellahi R (2016) Heat transfer analysis on peristaltically induced motion of particle–fluid suspension with variable viscosity: clot blood model. *Comput Methods Progr Biomed* 137:115–124
- Bhatti MM, Zeeshan A, Ellahi R, Ijaz N (2017) Heat and mass transfer of two-phase flow with Electric double layer effects induced due to peristaltic propulsion in the presence of transverse magnetic field. *J Mol Liquids* 230:237–246
- Bhatti MM, Zeeshan A, Ellahi R (2017) Simultaneous effects of coagulation and variable magnetic field on peristaltically induced motion of Jeffrey nanofluid containing gyrotactic microorganism. *Microvasc Res* 110:32–42
- Ellahi R, Shivanian E, Abbasbandy S, Rahman SU, Hayat T (2012) Analysis of steady flows in viscous fluid with heat/mass transfer and slip effects. *Int J Heat Mass Transf* 55(23):6384–6390
- Ellahi R, Hassan M, Zeeshan A (2015) Shape effects of nanosize particles in Cu- H₂O nanofluid on entropy generation. *Int J Heat Mass Transf* 81:449–456
- Ellahi R, Zeeshan A, Hassan M (2016) Particle shape effects on Marangoni convection boundary layer flow of a nanofluid. *Int J Numer Methods Heat Fluid Flow* 26(7):2160–2174
- Elshehawey EF, Eldabe NT, Elghazy EM, Ebaid A (2006) Peristaltic transport in an asymmetric channel through a porous medium. *Appl Math Comput* 182(1):140–150
- Eytan O, Elad D (1999) Analysis of intra-uterine fluid motion induced by uterine contractions. *Bull Math Biol* 61(2):221–238
- Fung FC, Yih CS (1968) Peristaltic transport. *J Appl Mech* 85:669–675
- Hayat T, Tanveer A, Alsaadi F, Alotaibi ND (2015) Homogeneous-heterogeneous reaction effects in peristalsis through curved geometry. *AIP Adv* 5(6):067172
- Hayat T, Zahir H, Tanveer A, Alsaedi A (2016) Numerical study for MHD peristaltic flow in a rotating frame. *Comput Biol Med* 79:215–221
- Hayat T, Tanveer A, Alsaedi A (2016) Mixed convective peristaltic flow of Carreau–Yasuda fluid with thermal deposition and chemical reaction. *Int J Heat Mass Transf* 96:474–481
- Hayat T, Bibi S, Rafiq M, Alsaedi A, Abbasi FM (2016) Effect of an inclined magnetic field on peristaltic flow of Williamson fluid in an inclined channel with convective conditions. *J Magn Magn Mater* 401:733–745
- Hayat T, Shafique M, Tanveer A, Alsaedi A (2016) Magnetohydrodynamic effects on peristaltic flow of hyperbolic tangent nanofluid with slip conditions and Joule heating in an inclined channel. *Int J Heat Mass Transf* 102:54–63
- Hayat T, Farooq S, Ahmad B, Alsaedi A (2017) Effectiveness of entropy generation and energy transfer on peristaltic flow of Jeffrey material with Darcy resistance. *Int J Heat Mass Transf* 106:244–252

- Hina S, Hayat T, Asghar S, Hendi AA (2012) Influence of compliant walls on peristaltic motion with heat/mass transfer and chemical reaction. *Int J Heat Mass Transf* 55(13):3386–3394
- Javed M, Hayat T, Mustafa M, Ahmad B (2016) Velocity and thermal slip effects on peristaltic motion of Walters-B fluid. *Int J Heat Mass Transf* 96:210–217
- Khaled ARA, Vafai K (2003) The role of porous media in modeling flow and heat transfer in biological tissues. *Int J Heat Mass Transf* 46(26):4989–5003
- Latham TW (1966) Fluid motion in a peristaltic pump. MIT, Cambridge
- Maiti S, Misra JC (2011) Peristaltic flow of a fluid in a porous channel: a study having relevance to flow of bile within ducts in a pathological state. *Int J Eng Sci* 49(9):950–966
- Maiti S, Misra JC (2012) Peristaltic transport of a couple stress fluid: some applications to hemodynamics. *J Mech Med Biol* 12(3):1250048
- Misra JC, Mallick B, Sinha A (2018) Heat and mass transfer in asymmetric channels during peristaltic transport of an MHD fluid having temperature-dependent properties. *Alex Eng J* 57(1):391–406
- Mustafa M, Abbasbandy S, Hina S, Hayat T (2014) Numerical investigation on mixed convective peristaltic flow of fourth grade fluid with Dufour and Soret effects. *J Taiwan Inst Chem Eng* 45(2):308–316
- Nadeem S, Akram S (2010) Peristaltic flow of a Williamson fluid in an asymmetric channel. *Commun Nonlinear Sci Numer Simul* 15(7):1705–1716
- Nadeem S, Akram S (2010) Influence of inclined magnetic field on peristaltic flow of a Williamson fluid model in an inclined symmetric or asymmetric channel. *Math Comput Model* 57(1):107–119
- Narayan R, Goswamy R (1994) Subendometrial-myometrial contractility in conception and non-conception embryo transfer cycles. *Ultrasound Obstet Gynecol* 4:499–504
- Raissi P, Shambooli M, Sepasgozar SME, Ayani M (2016) Numerical investigation of two-dimensional and axisymmetric unsteady flow between parallel plates. *Propul Power Res* 5(4):318–325
- Ramesh K (2016) Effects of slip and convective conditions on the peristaltic flow of couple stress fluid in an asymmetric channel through porous medium. *Comput Methods Progr Biomed* 135:1–14
- Ramesh K (2016) Influence of heat and mass transfer on peristaltic flow of a couple stress fluid through porous medium in the presence of inclined magnetic field in an inclined asymmetric channel. *J Mol Liquids* 219:256–271
- Reddy MVS, Rao AR, Sreenadh S (2007) Peristaltic motion of a power-law fluid in an asymmetric channel. *Int J Non Linear Mech* 42(10):1153–1161
- Shapiro AH (1967) Pumping and retrograde diffusion in peristaltic waves. In: Proceedings of the workshop ureteral reftm children, National Academy of Science, Washington, DC
- Shapiro AH, Jafrin MY, Weinberg SL (1969) Peristaltic pumping with long wavelengths at low Reynolds number. *J Fluid Mech* 37:799–825
- Shirvan KM, Mamourian M, Mirzakanlari S, Ellahi R (2017) Numerical investigation of heat exchanger effectiveness in a double pipe heat exchanger filled with nanofluid: a sensitivity analysis by response surface methodology. *Powder Technol* 313:99–111
- Shit GC, Ranjit NK (2016) Role of slip velocity on peristaltic transport of couple stress fluid through an asymmetric non-uniform channel: application to digestive system. *J Mol Liquids* 221:305–315
- Shit GC, Ranjit NK, Sinha A (2016) Electro-magnetohydrodynamic flow of biofluid induced by peristaltic wave: a non-Newtonian model. *J Bionic Eng* 13(3):436–448
- Srinivas S, Pushparaj V (2008) Non-linear peristaltic transport in an inclined asymmetric channel. *Commun Nonlinear Sci Numer Simul* 13(9):1782–1795
- Srinivasacharya D, Hima Bindu K (2016) Entropy generation in a porous annulus due to micropolar fluid flow with slip and convective boundary conditions. *Energy* 111:165–177
- Stokes VK (1966) Couple stresses in fluids. *Phys Fluids* 9(9):1709–1715
- Tripathi D (2013) Study of transient peristaltic heat flow through a finite porous channel. *Math Comput Model* 57(5):1270–1283
- Tripathi D, Beg OA (2014) A study on peristaltic flow of nanofluids: application in drug delivery systems. *Int J Heat Mass Transf* 70:61–70
- Tripathi D, Beg OA (2015) Peristaltic transport of Maxwell viscoelastic fluids with a slip condition: homotopy analysis of gastric transport. *J Mech Med Biol* 15(3):1550021
- Tripathi D, Beg OA, Gupta PK, Radhakrishnamacharya G, Mazumdar J (2015) DTM simulation of peristaltic viscoelastic biofluid flow in asymmetric porous media: a digestive transport model. *J Bionic Eng* 12(4):643–655
- Turan I, Kitapcioglu G, Goker ET, Sahin G, Bor S (2016) In vitro fertilization-induced pregnancies predispose to gastroesophageal reflux disease. *United Eur Gastroenterol J* 4(2):221–228
- Wang Y, Ali N, Hayat T, Oberlack M (2011) Peristaltic motion of a magnetohydrodynamic micropolar fluid in a tube. *Appl Math Model* 35(8):3737–3750

Publisher's Note Springer Nature remains neutral with regard to jurisdictional claims in published maps and institutional affiliations.